ROCK MECHANICS ASPECTS OF BLOWOUT

SELF-CONTAINMENT

A Thesis

by

BABAK AKBARNEJAD NESHELI

Submitted to the Office of Graduate Studies of
Texas A&M University
in partial fulfillment of the requirements for the degree of

MASTER OF SCIENCE

August 2006

Major Subject: Petroleum Engineering

ROCK MECHANICS ASPECTS OF BLOWOUT

SELF-CONTAINMENT

A Thesis

by

BABAK AKBARNEJAD NESHELI

Submitted to the Office of Graduate Studies of
Texas A&M University
in partial fulfillment of the requirements for the degree of

MASTER OF SCIENCE

Approved by:

Chair of Committee,	Jerome J. Schubert
Committee Members,	Peter P. Valkó
	Charles Aubeny
Head of Department,	Stephen A. Holditch

August 2006

Major Subject: Petroleum Engineering

ABSTRACT

Rock Mechanics Aspects of Blowout Self-Containment.

(August 2006)

Babak Akbarnejad Nesheli, B.S., Tehran University

Chair of Advisory Committee: Dr. Jerome J. Schubert

A blowout is an uncontrolled flow of reservoir fluids into the wellbore to the surface, causing serious, sometimes catastrophic, problems in different types of petroleum engineering operations. If the formation's strength is low and the pore pressure is high, bridging can be a very effective method for blowout containment. In this method, the formation caves into the open hole or onto the casing and stops the flow of the formation's fluid, either naturally or intentionally. This method can be effective in deepwater blowouts where the formation has high pore pressure and considerable shale intervals with low strength.

In this research, wellbore stability and fluid flow performance subroutines have been developed with Visual Basic for Applications (VBA) programming. By integrating the subroutines together, we made a simulation tool to predict wellbore stability during blowouts and, consequently, predict wellbore bridging during normal and blowout situations. Then we used a real case in the country of Brunei to investigate a field case of a bridged wellbore to validate the simulator. In addition to the field case, we used GMI SFIB 5.02, a wellbore stability software, to provide validation.

In the final part of this research we studied the effect of water depth in bridging tendency during blowout for the deepwater Gulf of Mexico (GOM). Since we could not find any real data in this area, we used general trends and correlations related to the GOM. The results of our study showed that water depth delays the occurrences of breakout in the wellbore during blowouts (i.e. for greater depth of water, wellbore

collapse occurs farther below the mudline). However, the depth in which collapse occurs is different for different maximum horizontal stress amounts.

DEDICATION

I would like to dedicate this thesis to my family. Thinking of them always gives me energy and passion.

ACKNOWLEDGMENTS

I would like to first thank my advisor, Dr. Jerome J. Schubert, for his advice. I appreciate his giving me the opportunity to work on this project.

I would also like to thank Dr. Peter P. Valkó for being on my committee and answering my questions. Also, I thank Dr. Charles Aubeny for being on my committee as a non-petroleum engineer.

Thanks to all the faculty and staff at Texas A&M University who helped provide an excellent education within the field of petroleum engineering.

Last but not least, I want to thank my dear family and friends, near and far, for being there for me throughout the years.

TABLE OF CONTENTS

LIST OF FIGURES

CHAPTER I
INTRODUCTION

1.1 Overview

Blowout control is one of the most challenging problems in exploration, drilling, and production operations. If the well experiencing a blowout has significant openhole intervals, it is possible that the well will bridge over downhole (seal itself with rock fragments from collapsing formations) and intervention efforts will be averted.

We can induce bridging or it may happen by itself. To induce wellbore bridging, we may open the blowout preventer (BOP) or diverting stack to allow entry of reservoir fluid, which results in high wellbore fluid velocities and pressure profile changes along the wellbore. This technique can be a very effective method for controlling offshore blowouts where the formation strength is low and pore pressure is high.

There are two basic theories about the quality of the bridging procedure.[1, 2] The first theory has a geomechanical base and says if exposed rocks or formation cannot support the pressure differentials caused by rapid and uncontrolled change in the fluid pressure both within the wellbore and within the formation, the formation caves into the open hole or the casing and stops the fluid flow. In the second theory, the most important factors in stoping the blowout and fluid flow are solids which are produced in the formation during the blowout. Backpressure caused by the high density of transported mixture (during the blowout, the formation produces more solids and the mixture's density increases with time) and additional friction can exceed the declining formation pressure and stop the fluid flow.

To choose the best plan for preventing the blowout in the industry, we usually develop several "blowout scenarios." A simulator that can estimate the wellbore stability under blowout conditions (which the existing simulators are not able to do) can be used as an engineering tool for contingency and blowout containment planning.

This thesis follows the style and format of *SPE Drilling and Completion.*

Wellbore hydraulics, reservoir performance, solids transportation, and rock mechanics are the most important parts of the wellbore bridging study. This research focused on the rock mechanics aspect and investigated the stress state and rock failure in the near-wellbore region.

Whenever the stresses exceed the rock strength, rock instability occurs. Therefore, any rock stability study and stress analysis must choose a failure criterion and define the boundary conditions.

In petroleum engineering, stresses around the wellbore are mostly calculated with analytical models which are based on linear elastic behavior of rock. In the linear elastic study, the state of stress and strain is defined by a six-by-six material properties matrix and beyond the elastic limit will be plastic deformation.

Most of the rock stability studies assume that the rock is isotropic, homogeneous, and linearly elastic. Because the application is easy and yields very fast computational results, the linear-elastic analysis is the most common approach. Therefore most of the current available simulators are based on linear-elastic models for well path optimization and safe mud window design.

More advanced elasto-plastic models can lead to more realistic results. These rigorous elasto-plastic models are very sensitive to the input parameters and need well-defined rock properties to be obtained. However in most practical circumstances it is not possible to obtain all the necessary input parameters and a simplistic conservative elastic analysis is the best choice for most situations. Therefore, it is more desirable to simplify the failure criteria, leading to wide application of the Mohr-Coulomb criterion.

1.2 Blowouts

1.2.1 Definitions

According to Salvato and Flak,[3] a blowout is a sudden, accidental, uncontrolled, and continuous expulsion of drilling fluid above the surface of an oil or gas well, followed by continuous and uncontrolled flow of oil, gas, or water as subterranean pressures cause the well to go completely out of control.

1.2.2 Surface Blowouts

It is always important to be aware of water depth effect on an ultradeepwater blowout[4]. If the drillpipe shears, during the blowout, a significant hydrostatic pressure will be removed. The impact of seawater hydrostatic pressure at the mudline can add a significant backpressure to broach blowout flow, which increases flowing bottomhole pressure and also reduces formation drawdown and flow rate. This will reduce the bridging tendency.

Riser margin loss can cause even more risks in deepwater conditions.[5] Sometimes if an upper zone breaks down and cross-flow begins, a kick from riser margin loss can cause an underground blowout. Consequently, the lower-density blowout fluids will remove the mud from the casing and the BOP's pressure will increase. If the open part of the hole bridges during this period, the drillpipe can kick while bottomhole pressure reaches shut-in conditions. Choe[6] introduced several concepts of riserless drilling and compared it with similar conditions in conventional marine riser drilling in deepwater applications.

1.2.3 Underground Blowouts

Barnhill and Adams[7] have defined an underground blowout as the uncontrolled flow of formation fluid into formation through fractures in the wellbore (**Fig. 1.1**). Basically, an underground blowout involves a significant downhole flow of formation fluids from the flowing zone with a higher pressure to the charged/loss zone, which is one of the lower-pressure zones.
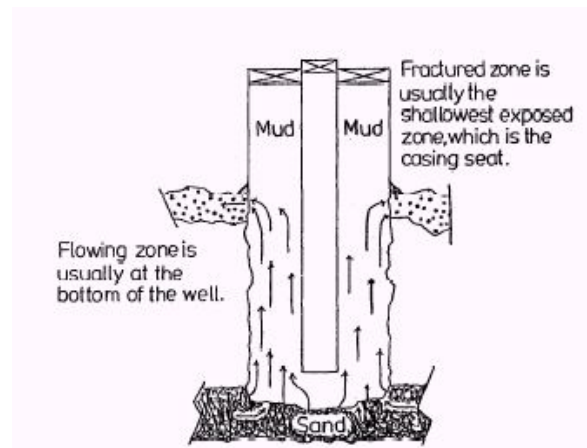
Fig. 1.1—Underground blowout, (from Branhill and Adams[7]).

Underground blowouts can be very dangerous and can potentially turn into surface blowouts at shallow casing depths. However, low kick tolerance and minimal differential between pore pressure and fracture extension pressure increases the probability of underground blowouts in ultradeepwater operations.

1.2.4 Shallow Gas Blowouts

According to Adams and Kuhlman's[1] definition, a shallow gas blowout is related to either low fracture gradient or gas migration through cement. The first case occurs in shallow depths where the low fracture gradient makes it almost impossible to control kicks with conventional shut-in techniques. These shallow depths range from the surface to the conductor or surface casing setting point. The latter case occurs in openhole situations below the conductor or surface casing or behind the surface casing. A common example of this type of shallow gas blowout is when the gas migration causes a blowout through the annulus of the surface conductor casing or intermediate surface casing.

1.2.5 Blowout Statistics

Based on statistical data, just 20% of all blowouts have a duration of more than one week.[1] A study[8] of 53 blowouts in the Outer Continental Shelf (OCS) has shown that, 24

of these blowouts bridged, and 14 of these bridged blowouts had a duration of 1 to 12 hours. In the worst case, bridging time was about one month.

Skalle, Jinjun, and Podio[9], statistically analyzed a database of about 1,120 blowout events from the gulf coast and adjoining states covering the period of 1960-1996. They categorized blowing fluid into 11 groups. In the OCS, 79% of blowouts are pure gas. Liquids blowouts account for 11%, and 10% of blowouts contain a mixture of gas and liquids. However in Texas, the blowout occurrences caused by pure gas, liquids, and mixtures of gas and liquids are 52%, 8%, and 40% respectively. It is clear that gas is the most dangerous kick fluid. This means that from 89% to 92% of the blowouts in Texas and the OCS contain some form of gas. This study also showed that in Texas, 189 blowouts took place reportedly in sand formations, 80 in lime, and 11 in other formations.

A cumulative percentage of blowouts vs. duration is shown in **Fig. 1.2**.[9] The majority of the events were of short duration; about half of the occurrences were controlled within one day in the OCS and in Texas, and about 80% of the blowouts stopped blowing within one week.
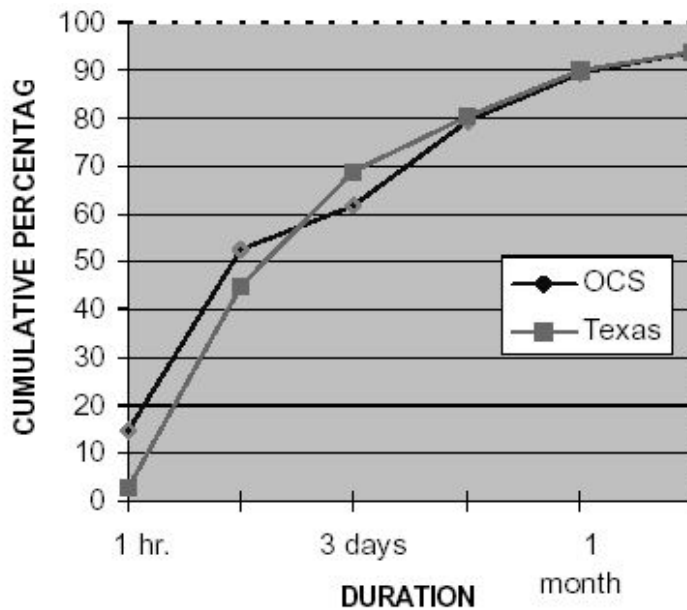
Fig. 1.2— Blowout vs. duration (from Skalle *et al.*[9]).

Skalle and Podio[8] suggest that blowout probability is much higher in deeper wells because both the drilling exposure time and the formation pressure are higher. Furthermore, Whylie and Visram[10] found additional parameters that increase the blowout probability in deeper wells, including longer openhole sections, more tripping time, and increased risk of lost circulation.

Skalle, Jinjun, and Podio[9] introduced eight different methods of blowout control: collapse of openhole wellbore (bridging), closing the BOP, pumping cement slurry (cement), capping, depleting small reservoirs, installing new equipment, pumping mud, and drilling relief wells. **Fig. 1.3**[9] clearly shows that in the OCS, bridging is the most common method of control with 39.6% and killing with weighted mud ranks second with 19%. Conversely, in Texas the most common method is mud with 41%, while bridging ranks second with 19%.
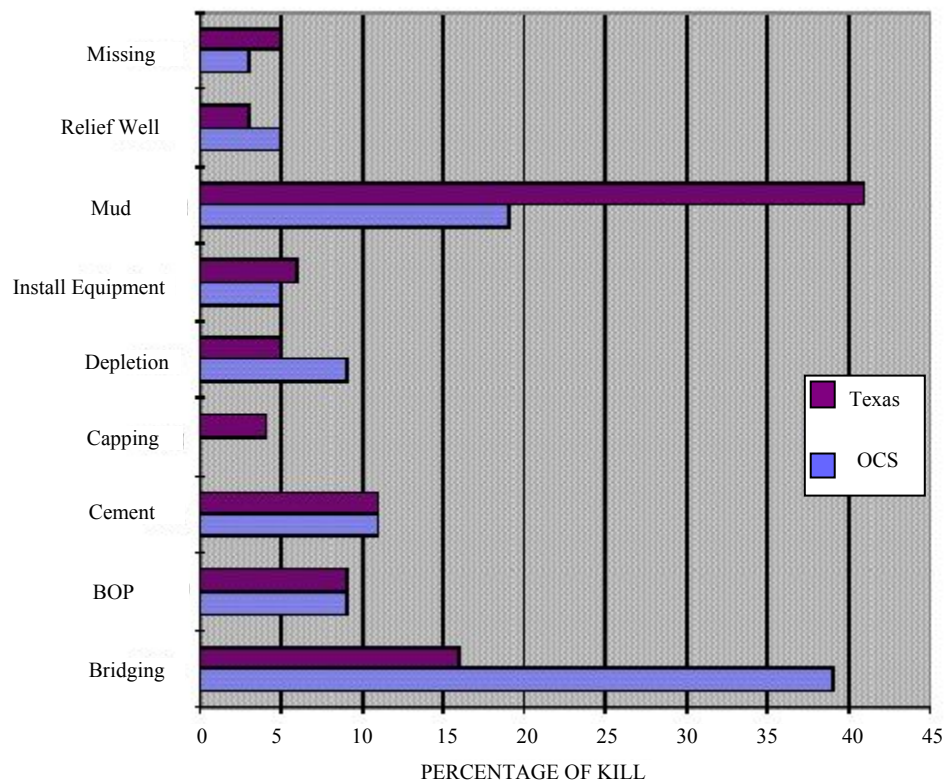
Fig. 1.3—Different blowout control methods in Texas and the OCS (from Skalle *et al.*[9]).

Flak[4] found that natural well bridging would shut off most blowouts, and ultradeepwater blowout risk is mitigated by low formation strength. Adams and Kuhlman[11] affirm that natural formation bridging stops many shallow blowouts. The formation around the wellbore collapses and seals the flow path. They found that bridging typically occurs within 24 hours after the well blows out, which generally corresponds with Skalle, Jinjun, and Podio.[9] If the well does not bridge within 24 hours, it is likely to blow for an extended time or until it is mechanically killed.

1.3 Bridging

1.3.1 Mechanisms

Whenever a wellbore caves into the open hole, restrictions in the flow path stop the flow, and bridging occurs. If the well is not open hole and we have casing annulus blowout, the formation caves in on the casing and stops the flow.

We can study the bridging as the part of the well-developed problem of borehole instability. Mechanical effects, chemical effects, or a combination of both can lead to wellbore instability. Shallow casing strings, formation instability under drawdown situations, gas blowout fluids, high flow rates, shallow water depths, and saltwater flows in deeper wells are factors generally found in bridging situations. Also lightweight fluids, borehole erosion caused by high annular velocities, and chemical interactions between the lightweight fluids and water-sensitive shales often increase wellbore instability.[12]

Several failure mechanisms can lead to bridging:

1. High fluid flow rates can drag the rock fragments into the wellbore and up the well; this is the most common cause for bridging.[11] Opening the BOP/diverting stack is an active bridging technique in this situation as it allows accelerated entry of reservoir fluids and subsequent bridging.

2. For the flowing well, the rock may become unstable as pressure drops during the formation drawdown, and the formation may cave or bidge.[11]

3. Pore pressure in faults or bedding joints may increase as abnormal fluid pressure migrates from deeper gas or water-bearing layers channeled through damaged cementation. Therefore, the released effective normal stress on faults can induce shear mode displacements and casing deformation.

4. If the flow from a blowout is allowed to continue, mechanical heaving or chemical sloughing can bridge the blowing hole.[7]

1.3.2 Surface Venting

Sometimes it is possible to induce the bridging by decreasing the flowing bottomhole pressure (FBHP) via surface venting.[2] Flowing zone permeability and wellbore fracture pressure are the controlling parameters here. FBHP can be high if the flowing formation has a high permeability; on the other hand, high wellbore fracture pressure can limit the FBHP needed to support exposed shales. Thus, a high-rate surface venting can drop FBHP below fracture pressure and cause bridging.

1.3.3 Production Rate

El-Sayed[13] studied the stress distribution and stability around a horizontal wellbore as a function of pressure drawdown and overburden stress. He developed an equation to calculate the maximum production rates from the open hole without sand production or wellbore collapse. This equation takes into account the effect of well depth and the length of the horizontal displacement. It can also be applied to calculate the effective borehole diameter of the horizontal well that estimates sand production.

In deep water, the differential between the hydrostatic pressure developed within the riser mud column and the surrounding seawater is called the "riser margin." Flak and Boots[5] show that the loss of riser margin results in a dramatic loss in applied hydrostatic pressure within the borehole. The loss is greater in deeper water. They describe the possible hole response and declare that the following circumstances can be expected in the GOM: small kick flowed into wellbore (kick volume limited by compressibility of mud and hole ballooning unless a leak develops or the open hole breaks down); hole

likely collapsed around drill string (in GOM deepwater); well likely bridged from hole collapse (in GOM deepwater); trapped pressure under BOPs may bleed-off if well bridges.

1.3.4 Temperature

The effect of thermal stresses on borehole stability has been investigated by Maury and Guenot.[14] Their investigation showed that cooling or heating by 1°C induces a 0.4 to 1 MPa tensile or compressive stress, depending on the rigidity of the rock. A change of 25°C in temperature is common while drilling at a depth of 2,000 to 3,000m and can reach up to 60 to70°C, which can induce several 10s of MPa stress. Thermal effects during blowouts can have great effects on borehole collapse. Therefore, it is very important to consider the effect of thermal induced stress in any stress analysis.

1.4 Stress Analysis

Based on geomechanical concepts, rock instability occurs when stresses exceed rock strength. Therefore, stress analysis is the basic requirement for any rock stability studies, and consequently, it is necessary to choose a failure criterion implemented with geometry, constitutive law, and boundary condition.

Several equations are used for stress analysis and calculation. All of these equations follow the consideration of material laws. The three main classic idealizations of real material behavior are the elastic,[15] plastic,[13] and poroelastic.[16] In any stress and failure analysis, it is always desirable to know what simplification should be made. However, there is no final answer for this question and the level of simplification that should be made in any analysis relates more to art than to the science of rock mechanics and engineering design.[17]

In petroleum engineering most of the analytical models for calculating the stresses around the borehole are based on linear elastic models, and they are widely used in industry.[18, 19] In the linear elastic models, a six-by-six material property matrix can be

used to describe the relationship between the stresses and strains based on material law. Any deformation beyond the elastic limit will be categorized as plastic deformation.[20, 21]

The most common assumptions about rock are isotropy, homogeneity, and linear elasticity. Because of the ease of application, the linear-elastic models are the most common approaches. Gray[22] showed that linear-elastic models yield very fast computational results. Awal[23] found that analytical models based on the linear elastic behavior of rock are excellent tools for designing and optimizing the trajectory of the borehole. Therefore, linear elastic models are the dominant models in most currently available simulators. For instance, Van Oort, Nicholson, and D'Agostino[24] applied linear elastic models as quick screening tools for well-path optimization. Mohiuuddin, Awal, and Khan[25] designed safe mud weight windows using linear elastic models. Garrouch and Ebrahim[26] suggest employing a linear-elastic model for calculating the stresses around the wellbore with different inclination angles in various stress regimes. Moos's[27] model assumption is that the rock in which borehole drilling occurs is elastic and isotropic.

In some conditions more advanced elasto-plastic models give more accurate predictions. These models[28] suggest that after reaching the peak stress, rock still has residual strength and is connected to the wellbore wall.

The rigorous elasto-plastic modeling techniques can be used when well-defined rock properties can be obtained, although these models need detailed data about well geometry, rock properties, formation stress state, drilling experiences, etc. A number of researchers have tried to model the complex behavior of rock around boreholes. For example, Van Oort, Nicholson, and D'Agostino[24] provided a numerical finite-element elasto-plastic model for mud weight prediction, which is more realistic and less conservative than previous models. They calibrated and validated their model using several hundred wells drilled by Shell worldwide.

Nevertheless, in real-life petroleum engineering circumstances, the poor definition of key input parameters suggests that the best model still is a simplistic conservative elasto-plastic analysis.

The theory of poroelasticity efficiently describes the temporal material responses to fluid flow. Terzaghi[29] has developed the general theory of a porous material containing a compressible fluid for one-dimensional consolidations. The same theory has been developed by Biot[30] for three-dimensional consolidations. The more advanced model has been provided by Frydman and Fountoura,[31] where they applied analytical poroelastic solutions. By applying this model, they predicted the stability of an inclined wellbore drilled through a poroelastic porous material. Their boundary conditions included an in-situ stress field, a virgin pore pressure, and internal wellbore pressure.

In all of these cases, the numerical solution of the problem is usually obtained with the assumption of highly idealized pressure behavior, such as a step function[32], at the boundaries. The real boundary pressures and stresses encountered during oil and gas well unloading show more complex behavior with time.

1.4.1 Strength Criteria

If rock is loaded to its elastic limit under a number of different combinations of principal stresses, the resulting locus of points plotted in stress space defines the strength of the material as a mathematical function. This function is the failure criterion, and its parametric form is often selected according to some empirical rule. Several failure criteria have been suggested, but none of the simple rules are completely consistent with experimentation.

The Mohr-Coulomb and Drucker-Prager criteria have the most application. Garrouch and Ebrahim[26] have compared the results of both Mohr-Coulomb and Drucker-Prager failure criteria for estimating the drilling fluid density at which the wellbore would collapse. They found that the Mohr-Coulomb failure criterion overestimates mud densities required to prevent wellbore collapse. However, Mohiuuddin and Khan[25]observed that three criteria (Mohr-Coulomb, and middle and inner Drucker-Prager) predict mud weights in a very close range and give good estimates of mud weights.

Wilson *et al.*[33] presented several examples of the application of geomechanical analysis using both deterministic and probabilistic methods. This model was adapted to include slippage on bedding planes, as defined by a Mohr-Coulomb frictional surface. This analysis also includes the interaction between the well trajectory, in-situ stresses, and relative strength of the intact formation and bedding planes.

Wang and Lu[34] used a special criterion based on critical effective plastic strain to determine the onset of borehole collapse and sand prediction. They claim that the criterion is superior to the conventional stress/strength criterion as the peak stress is often associated with neither the wellbore collapse nor sand production.

Several theoretical investigations and practical experiences[28] confirm the importance of fluid pore pressure evolution in controlling formation stability. The direct effect of low bottomhole pressures or pore fluid pressure is an increase in shear stresses acting around the circumference of a well, which leads to shear failure. Some other factors which affect the failure behavior are intermediate principal stress, stress gradients, stress paths, and strain rate.

1.4.2 Advanced Models

Moos and Zoback[35] proposed an interactive borehole-stability model. This two-step process consists of the determination of stress from failure observations in existing wells and then using the results for the prediction of proposed wells while drilling and later during the production phase. Wiprut and Zoback[36] used another borehole stability approach based on previous knowledge of the vertical stress, the minimum horizontal stress, the pore pressure, the mud weight, and the change in temperature at the borehole wall during drilling operations.

In a more advanced model, based on the formation and fluid type, the chemical rock/fluid interaction might be considered as well as mechanical interaction. The differential pressure between the wellbore pressure and the formation pore pressure, and also the differential chemical potential between the drilling fluid and the formation pore fluid, can cause the movement of water in and out of the rocks.[37]

Van Oort, Nicholson, and D'Agostino[24] developed a model for special conditions that considered the effects of thermal stresses and chemical interactions on the wellbore stability. Hemphill and Tare[37] categorized three mechanisms affecting the time-dependent chemical instability of drilling fluid: elevation of near-wellbore pore pressure as mud pressure invades, elevation of swelling pressure, and chemical alteration and weakening of shale matrix cementation bonds.

Ghassemi, Diek, and Santos[38] proposed an analytical solution of a set of field equations to establish a coupled chemo-mechanical model. These field equations are associated with solute mass fraction, pore pressure, and solid displacements. They concluded that osmosis alters the pore pressure and the total tangential stress around the borehole, and an increase in mud salinity can improve borehole stability. Frydman and Fontoura[31] developed a more robust, chemical-hydro-mechanical model of an inclined wellbore in a saturated porous medium subjected to an anisotropic stress field and a nonisothermal condition.

CHAPTER II

ROCK MECHANICAL CONCEPTS

2.1 Overview

2.1.1 Poroelasticity

Poroelasticity in the near- wellbore condition explains how the pore pressure, p_p, effect on acting stresses and strains in grain-to-grain rock contact. The concept of effective stress was introduced by Terzaghi[39]and then modified by Biot.[40] The effect of pore pressure in the acting stresses and strains is measured by the Biot constant, α, as below:

$$\sigma_{ij}^{'} = \sigma_{ij} - \alpha p_p \quad \text{, and} \quad \text{...} (2.1)$$

$$\alpha = 1 - \frac{C_r}{C_b}, \quad \text{...} (2.2)$$

where;

$\sigma_{ij}{'}$ = Effective stress

σ_{ij} = Total stress

α = Biot constant

p_p = Pore pressure

C_r = Rock matrix compressibility

C_b = Bulk compressibility

According to Eq. 2.2 for rocks with no porosity, the Biot constant,α, becomes zero ($C_r = C_b$). However, if the rock has high porosity, the matrix compressibility will be much smaller than the bulk compressibility, and the Biot constant will approach one.

2.1.2 Elastic Rock Properties

Elastic rock properties are categorized as static and dynamic. Static elastic constants, which may also be known as quasistatic constants, are usually obtained from the lab test, in which rock is being underloaded in a testing machine. On the other hand, dynamic

elastic constants usually are determined from the measurement of wave velocity in the rock. If we consider the material as ideally elastic, the static and dynamic constants will be the same. For materials like rocks, this cannot be a proper assumption; however, at high confining pressure the stress-strain relation becomes more linear and there is a better consistency between them. Generally, the elastic constant values obtained by static methods are lower than those obtained by dynamic techniques.[41]

2.1.3 Young's Modulus (E)

For static condition, Young's modulus simply relates the axial strain to axial stress for isotropic, linearly elastic materials while performing a sample tension or compression test[42]:

$$\sigma_{xx} = E_s \, \varepsilon_{xx}, \quad \text{... (2.3)}$$

where;

σ_{xx} = Normal stress in x direction

E_s = Static Young's modulus, and ε_{xx} is the strain in x direction.

The static Young's modulus is proportional to the stiffness of the sample, and the higher the Young's modulus, the harder it is to deform the sample under uniaxial loading.

Based on the elastic wave theory, the compressional and shear wave velocity are related to the dynamic Young's modulus as shown in Eq. 2.4[43]:

$$E_D = \rho_b V_p^2 \frac{(1+v)(1-2v)}{1-v} = \rho_b V_s^2 \frac{3V_p^2 - 4V_s^2}{V_p^2 - V_s^2}, \quad \text{...................................... (2.4)}$$

where;

E_D = Dynamic Young's modulus

ρ_b = Bulk density

V_p = Compressional wave sonic velocity

v = Poison's ratio

V_s = Shear-wave sonic velocity

2.1.4 Poisson's Ratio (v)

Poisson's ratio is an elastic constant that is a measure of the compressibility of material perpendicular to applied stress, or the ratio of latitudinal to longitudinal strain.

In static measurements, Poisson's ratio relates the axial strain to transversal normal strain[42]:

$$\varepsilon_{yy} = \varepsilon_{zz} = -\nu\varepsilon_{xx} , \qquad\qquad\qquad (2.5)$$

where;

ε_{yy} = Strain in y direction

ε_{zz} = Strain in z direction

In general, Poisson's ratio has values between 0 and 0.5, but for rocks according to their properties and nature, it may change from 0.15 to 0.25.[41] Weak and highly porous rocks may have a Poisson's ratio very close to zero or even negative.

Based on the elastic wave theory, the compressional and shear wave velocity are also related to the dynamic Poisson's ratio as[43]:

$$\nu = \frac{V_p^2 - 2V_s^2}{2(V_p^2 - V_s^2)} , \qquad\qquad\qquad (2.6)$$

Dynamic Poisson's ratio may be shown in terms of transit times ($t_s=1/V_s$ and $t_c=1/V_p$):

$$\nu = \frac{\frac{1}{2}\left(\frac{t_s}{t_c}\right)^2 - 1}{\left(\frac{t_s}{t_c}\right)^2 - 1} , \qquad\qquad\qquad (2.7)$$

where;

t_s = Shear-wave transit time

t_c = Compressional wave transit time

2.2 Mohr-Coulomb Failure Criterion

The Mohr-Coulomb criterion is the most accepted failure criterion being used in wellbore-stability analysis. This criterion assumes that the yield occurrences in materials are frictional in nature. It also states that the shear stress that tends to cause shear yield on a plane in the rock is resisted by cohesion plus the product of a friction coefficient, and the normal stress acts on the yield plane. However, the weakness of this criterion is that it ignores the effect of intermediate principal stress. The Mohr-Coulomb criterion can be expressed in two basic forms, as[44]:

$$\tau = S_0 + \mu_f \sigma, \quad\quad\quad\quad\quad\quad\quad (2.8)$$

$$\sigma_1 = C_o + \sigma_3 \tan^2\left(45° + \frac{\phi_f}{2}\right), \quad\quad\quad\quad\quad\quad\quad (2.9)$$

where;

S_0 = Mohr-Coulomb cohesion of the material at zero confining pressure

τ = Shear stress necessary to cause failure across a plane resisted by S_0

μ_f = Coefficient of internal friction and differs from the μ, coefficient of sliding friction

σ = Normal stress acting on the yield plane

σ_1 = Maximum normal stress

σ_3 = Confining pressure

C_0 = Unconfined compressive strength

ϕ_f = Angle of internal friction

The angle of internal friction is related to the coefficient of internal friction as below:

$$\mu_f = \tan\phi_f, \quad\quad\quad\quad\quad\quad\quad (2.10)$$

Therefore, Eq. 2.8 and 2.9 might be stated as below:

$$\tan\left(45° + \frac{\phi_f}{2}\right) = \sqrt{1 + \mu_f^2} + \mu_f = \frac{1 + \sin\phi_f}{1 - \sin\phi_f}, \quad\quad\quad\quad\quad (2.11)$$

or

$$C_O = 2S_O \tan\left(45° + \frac{\phi_f}{2}\right), \quad \text{..} \text{(2.12)}$$

It is common in the Mohr-Coulomb criterion to show the status of the stability of a sample with a failure curve. In **Fig. 2.1**[45] the Mohr-Coulomb criterion is represented by a straight line of slope $\mu_f = \tan\phi_f$ and intercept S_0, on the τ axis. If the σ_1 - σ_3 circle touches the line of the Coulomb criterion, then brittle failure will occur. Failure takes place if the circle with a radius of σ_1 - σ_3 just touches the Mohr-Coulomb line. The failure curve is obtained experimentally and is an envelope of many Mohr circles corresponding to failure under a variety of confining pressure (σ_3) conditions. The straight line is the limiting equilibrium. Any circle below the straight line represents stable condition, and above the straight line is the unstable region.
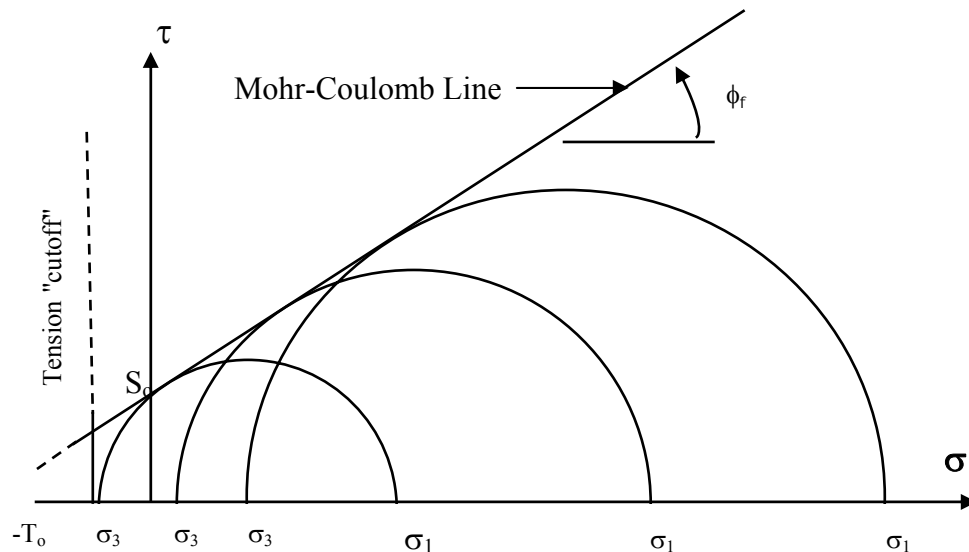
Fig. 2.1—The Mohr-Coulomb failure criterion (from Goodman[45]).

2.3 Modified-Lade Failure Criterion

The two most common failure criteria, Mohr-Coulomb and Drucker-Prager, are two extreme treatments of the intermediate principal stress.[46] In the Mohr-Coulomb criterion, the assumption is that intermediate principal stress has no influence on rock strength. On

the other hand, the Drucker-Prager criterion applies as much weight for intermediate principal stress as it applies for minimum and maximum principal stresses in failure of material. Intermediate principal stress has such an effect that it increases the strength of the material. In the Mohr-Coulomb criterion this effect is ignored, whereas the Drucker-Prager criterion applies an intermediate principal stress higher than the real one. This leads to an underestimation of rock strength by Mohr-Coulomb and an overestimation of rock strength in Drucker-Prager.

The modified-Lade failure criterion is a 3D rock-failure criterion proposed by Ewy,[46] which is a modification of a criterion originally developed by Lade.[47] The advantage of this criterion over Mohr-Coulomb and Drucker-Prager is that it properly describes the effect of the intermediate principal stress on rock strength, and in wellbore stability analysis it yields more realistic results. For this criterion having just two rock strength parameters like cohesion and friction angle will be sufficient.

The Lade criterion for failure of frictional materials is given below[47]:

$$\left(\frac{I_1^3}{I_3} - 27\right)\left(\frac{I_1}{P_a}\right)^m = \eta_1, \quad\text{...} \quad (2.13)$$

$$I_1 = \sigma_1 + \sigma_2 + \sigma_3 , \quad\text{...} \quad (2.14)$$

$$I_3 = (\sigma_1)(\sigma_2)(\sigma_3), \quad\text{...} \quad (2.15)$$

where;

I_1 = First stress invariant

I_3 = Third stress invariant

p_a = Atmospheric pressure

m = A material parameter

η_1 = A material parameter related to friction

σ_2 = Intermediate principal stress

Lade suggested that to handle materials with cohesion or a nonzero tensile strength the stress axes can be shifted into the tensile region by a dimensionless constant multiplied by p_a. Ewy set $m=0$ to have the Lade criterion for linear shear strength mode,

and then he defined S_1, which is a shift constant with units of cohesion. Then, he subtracted the pore pressure to handle effective stresses. Applying these modifications, and defining proper stress invariants I''_1 and I''_3, he obtained the following failure criterion[46]:

$$\frac{\left(I''_1\right)^3}{I''_3} = 27 + \eta\ , \dotfill (2.16)$$

$$I''_1 = \left(\sigma_1 + S_1 - p_p\right) + \left(\sigma_2 + S_1 - p_p\right) + \left(\sigma_3 + S_1 - p_p\right), \dotfill (2.17)$$

and

$$I''_3 = \left(\sigma_1 + S_1 - p_p\right)\left(\sigma_2 + S_1 - p_p\right)\left(\sigma_3 + S_1 - p_p\right), \dotfill (2.18)$$

where;

I''_1 = Modified first stress invariant

I''_3 = Modified third stress invariant

η = A material parameter related to friction

S_1 = A cohesion-like material parameter

p_p = Formation pore pressure

He also calculated I''_1 and I''_3 using the Eqs. 2.19 and 2.20 in place of Eqs. 2.17 and 2.18.:

$$I''_1 = \left(\sigma_{xx} + S_1 - p_p\right) + \left(\sigma_{yy} + S_1 - p_p\right) + \left(\sigma_{zz} + S_1 - p_p\right), \dotfill (2.19)$$

$$I''_3 = \left(\sigma_{xx} + S_1 - p_p\right)\left(\sigma_{yy} + S_1 - p_p\right)\left(\sigma_{zz} + S_1 - p_p\right) + 2\,\tau_{xy}\tau_{yz}\tau_{zx}$$
$$- \left(\sigma_{xx} + S_1 - p_p\right)\tau_{yz}^2 - \left(\sigma_{yy} + S_1 - p_p\right)\tau_{zx}^2 - \left(\sigma_{zz} + S_1 - p_p\right)\tau_{xy}^2, \dotfill (2.20)$$

where;

$\sigma_{xx} = \sigma_{yy} = \sigma_{zz} =$ Normal stresses in any Cartesian coordinates system

$\tau_{xy} = \tau_{yz} = \tau_{zx} =$ Shear stresses in any Cartesian coordinates system

We can also obtain S_1 and η from the Mohr-Coulomb cohesion S_0 and friction angle ϕ_f as shown below[46]:

$$S_1 = \frac{S_0}{\tan \phi_f} , \qquad \text{(2.21)}$$

$$\eta = 4 \tan^2 \phi_f \frac{\left(9 - 7 \sin \phi_f\right)}{\left(1 - \sin \phi_f\right)} , \qquad \text{(2.22)}$$

2.4 Stress State Around the Wellbore

2.4.1 In-Situ Stress Transformation

In any rock mechanical study, we characterized the formation by far-field in-situ stresses S_H, S_h, and S_v. According to **Fig. 2.2**,[41] γ is the inclination angle and ϕ is the azimuth of the borehole axis. For simplification, we define the coordinate system *(x', y',z')* in which the *x'* is parallel to the maximum horizontal stress, S_H, *y'* is parallel to minimum horizontal stress, S_h, and *z'*, is parallel to vertical stress, S_v. The origin coordinate system *(x, y, z)* is in the way that *z*-axis is parallel to the borehole axis, and *y*-axis is horizontal.
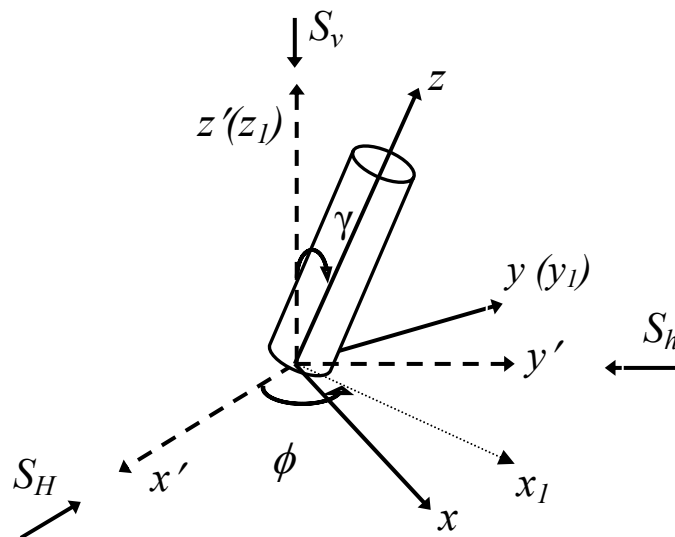
Fig. 2.2 – Geometry of an inclined borehole (from Fjaer *et al.*[41]).

To transform the coordinate system *(x′, y′, z′)* to the coordinate system *(x, y, z)* via the coordinate system *(x₁, y₁, z₁)* we have to:

- Rotate the coordinate system *(x′, y′, z′)* around the *z′*-axis at angle φ to the coordinate system *(x₁, y₁, z₁)*. Axis *z₁* is coincident with axis *z′*.

$$\begin{Bmatrix} x_1 \\ y_1 \\ z_1 \end{Bmatrix} = \begin{Bmatrix} \cos\phi & \sin\phi & 0 \\ -\sin\phi & \cos\phi & 0 \\ 0 & 0 & 1 \end{Bmatrix} \begin{Bmatrix} x' \\ y' \\ z' \end{Bmatrix},$$ .... (2.23)

where ϕ is the rotation angle.

- Rotate the coordinate system *(x₁, y₁, z₁)* around the y-axis at angle ϕ to the coordinate   system *(x, y, z)*.

$$\begin{Bmatrix} x \\ y \\ z \end{Bmatrix} = \begin{Bmatrix} \cos\gamma & 0 & -\sin\gamma \\ 0 & 1 & 0 \\ \sin\gamma & 0 & \cos\gamma \end{Bmatrix} \begin{Bmatrix} x_1 \\ y_1 \\ z_1 \end{Bmatrix},$$ .... (2.24)

where γ is the borehole inclination angle.

The directional cosine matrix between the coordinate system *(x, y, z)* and the coordinate system *(x′, y′, z′)* will be:

$$\begin{Bmatrix} x \\ y \\ z \end{Bmatrix} = \begin{Bmatrix} \cos\phi\cos\gamma & \sin\phi\cos\gamma & -\sin\gamma \\ -\sin\phi & \cos\phi & 0 \\ \cos\phi\sin\gamma & \sin\phi\sin\gamma & \cos\gamma \end{Bmatrix} \begin{Bmatrix} x' \\ y' \\ z' \end{Bmatrix},$$ .... (2.25)

The second-order stress tensor S_H, S_h, S_v expressed in the new coordinate system *(x, y, z)* can be obtained by applying the following transformation formula[42]:

$$[\sigma] = [l][S][l]^T,$$ .... (2.26)

where l is the directional cosine matrix between the *(x, y, z)* coordinate system and the coordinate system *(x′, y′, z′)*. The superscript *T* indicates the transpose of the matrix. The final transformation of the far-field stresses S_H, S_h, S_v in the coordinate system *(x′, y′, z′)* to the local coordinate system *(x, y, z)* is:

$$
\begin{Bmatrix} \sigma_{xx} \\ \sigma_{yy} \\ \sigma_{zz} \\ \tau_{xy} \\ \tau_{yz} \\ \tau_{xz} \end{Bmatrix} = \begin{Bmatrix} \cos^2\phi\cos^2\gamma & \sin^2\phi\cos^2\gamma & \sin^2\gamma \\ \sin^2\phi & \cos^2\varphi & 0 \\ \cos^2\phi\sin^2\gamma & \sin^2\phi\sin^2\gamma & \cos^2\gamma \\ -\sin\phi\cos\phi\cos\gamma & \sin\phi\cos\phi\cos\gamma & 0 \\ -\sin\phi\cos\phi\sin\gamma & \sin\phi\cos\phi\sin\gamma & 0 \\ \cos^2\phi\sin\gamma\cos\gamma & \sin^2\phi\sin\gamma\cos\gamma & -\sin\gamma\cos\gamma \end{Bmatrix} \begin{Bmatrix} S_H \\ S_h \\ S_v \end{Bmatrix}, \quad \text{............(2.27)}
$$

where;

S_H=Maximum horizontal stress,

S_h= Minimum horizontal stress,

S_v= Vertical stress,

Hence,

$$\sigma_{xx} = \left(S_H\cos^2\phi + S_h\sin^2\phi\right)\cos^2\gamma + S_v\sin^2\gamma, \quad \text{.................................... (2.28)}$$

$$\sigma_{yy} = S_H\sin^2\phi + S_h\cos^2\phi, \quad \text{.. (2.29)}$$

$$\sigma_{zz} = \left(S_H\cos^2\phi + S_h\sin^2\phi\right)\sin^2\gamma + S_v\cos^2\gamma, \quad \text{.................................... (2.30)}$$

$$\tau_{xy} = \frac{1}{2}\left(S_h - S_H\right)\sin2\phi\cos\gamma, \quad \text{.................................... (2.31)}$$

$$\tau_{xz} = \frac{1}{2}\left(S_H\cos^2\phi + S_h\sin^2\phi - S_v\right)\sin2\gamma, \quad \text{.. (2.32)}$$

$$\tau_{yz} = \frac{1}{2}\left(S_h - S_H\right)\left(\sin2\phi\sin\gamma\right), \quad \text{.................................... (2.33)}$$

2.4.2 Kirsch's Solution

According to Kirsch's[48] solution, in a homogenous and isotropic material the tangential stress distribution in the borehole wall is as shown in Eq. 2.34 to 2.36.

$$\sigma_{\theta\theta} = \left(\sigma_{xx} + \sigma_{yy} - P_m - 2(\sigma_{xx} - \sigma_{yy})\right)\cos2\theta - 4\tau_{xy}\sin2\theta, \quad \text{............................... (2.34)}$$

$$\sigma_{zz} = \sigma_{zz} - 2\nu\left(\sigma_{xx-}\sigma_{yy}\right)\cos2\theta - 4\nu\tau_{xy}\sin2\theta, \quad \text{.................................... (2.35)}$$

$$\tau_{\theta z} = 2\left(\tau_{yz}\cos\theta - \tau_{xz}\sin\theta\right), \quad \text{.................................... (2.36)}$$

where;

θ = Azimuthal angle measured from the x axis,

$\sigma_{\theta\theta}$ = Tangential stress,

σ_{zz} = Axial stress,

$\tau_{\theta z}$ = Shear stress in the cylindrical coordinate system acting in the θ, z,

The simplified form of Kirsch's solution under elastic conditions and in terms of effective stresses on the borehole wall is:

$$\sigma'_{rr} = p_m - \alpha p_p,$$ .... (2.37)

$$\sigma'_{\theta\theta} = \left(\sigma_{xx} + \sigma_{yy}\right) - 2\left(\sigma_{xx} - \sigma_{yy}\right)\cos 2\theta - 4\tau_{xy}\sin 2\theta - p_m - \alpha p_p,$$ .... (2.38)

$$\sigma'_{zz} = \sigma_{zz} - 2\nu(\sigma_{xx} - \sigma_{yy})\cos 2\theta - 4\nu\tau_{xy}\sin 2\theta - \alpha p_p,$$ .... (2.39)

$$\tau_{\theta z} = 2\left(-\tau_{xz}\sin\theta + \tau_{yz}\cos\theta\right),$$ .... (2.40)

where;

σ'_{rr} = Effective radial stress,

$\sigma'_{\theta\theta}$ = Effective tangential stress,

θ'_{zz} = Effective axial stress,

The effective principal stresses at any given point on the borehole wall are:

$$\sigma'_{rr} = p_m - \alpha p_p,$$ .... (2.41)

$$\sigma'_{t\max} = \frac{\left(\sigma'_{\theta\theta} + \sigma'_{zz}\right) + \sqrt{\left(\sigma'_{\theta\theta} - \sigma'_{zz}\right)^2 + 4\tau_{\theta z}^2}}{2},$$ .... (2.42)

$$\sigma'_{t\min} = \frac{\left(\sigma'_{\theta\theta} + \sigma'_{zz}\right) - \sqrt{\left(\sigma'_{\theta\theta} - \sigma'_{zz}\right)^2 + 4\tau_{\theta z}^2}}{2},$$ .... (2.43)

where;

σ'$_{t\text{max}}$= Maximum effective principal stress on the tangential plane of the borehole,

σ'$_{t\text{min}}$= Minimum effective principal stress on the tangential plane of the borehole,

2.5 In-Situ Stresses and Properties Correlations

In our simulator the outer boundary conditions are defined from the in-situ stress field. In-situ stress magnitude and orientation regarding wellbore trajectory are the most critical factors in wellbore collapse and instability. The first step in determining the in-situ stress model is to estimate the order of stresses. In a normal situation where there is no active tectonic force, the minimum principal far-field stress is horizontal and the maximum principal stress is vertical. However, if the area has active tectonic forces, the maximum principal stress can be horizontal. Generally, stress orientation can be determined from field observations, general geologic information, or the world stress map.

Several techniques have been developed to measure in-situ stresses. The most common methods are size of breakouts, hydraulic fracturing techniques, study of focal mechanisms of induced seismicity, overcoring, and core relaxation.

2.5.1 Vertical Stress

The vertical or overburden stress, S_v, at a depth of z is defined as the pressure exerted by the weight of the over laying formation and expressed as:

$$S_v = \int_0^z \rho_b(z)g\,dz,$$ .... (2.44)

where;

z = Depth,

ρ_b = Bulk density,

g = Acceleration due to gravity,

Bulk density, ρ_b, can be obtained from sonic logs. Eq. 2.45 shows the correlation of compressional velocity, and bulk density, ρ_b[49]:

$$\rho_b = 1.27V_p - 0.28V_p^2 + 0.0232V_p^3 + 0.327, \quad \text{..} \quad (2.45)$$

Bulk density may also be estimated by using Eq. 2.46 for porosity:

$$\rho_b = \varphi\rho_f + (1-\varphi)\rho_{ma}, \quad \text{..} \quad (2.46)$$

$$\varphi = \frac{t_c - t_{ma}}{t_f - t_{ma}}, \quad \text{..} \quad (2.47)$$

where;

t_{ma} = Compressional wave transit time of the matrix rock,

t_f = Compressional wave transit time of the saturating fluid rock,

ρ_f = Density of the saturating fluid,

ρ_{ma} = Matrix density of the rock,

φ = Porosity,

Usually, when there is no density log or sonic log, it is common to assume a vertical stress gradient of 1.0 psi/ft.

The static Young's modulus estimation for sandstones is given by[50]:

$$E_s = 0.0293E_D^2 + 0.4533E_D, \quad \text{..} \quad (2.48)$$

and for shales,

$$E_s = 0.0428E_D^2 + 0.233E_D, \quad \text{..} \quad (2.49)$$

Unconfined compressive strength, C_0, is the capacity of rock to withstand axially directed forces. Correlation of C_0 is given by[41]:

$$C_0 = 0.2787E_s^2 + 2.458E_s, \quad \text{..} \quad (2.50)$$

Manohar[51] has developed the following relations for obtaining angle of internal friction, ϕ_f, and cohesion, S_0, as a function of compressional sonic velocity, V_p:

$$\sin \phi_f = \frac{(V_p - 1)}{(V_p + 1)}, \quad \dots\dots\dots\dots\dots\dots\dots\dots\dots\dots\dots\dots\dots\dots\dots\dots\dots\dots\dots\dots \quad (2.51)$$

$$S_0 = \frac{5(V_p - 1)}{\sqrt{V_p}}, \quad \dots\dots\dots\dots\dots\dots\dots\dots\dots\dots\dots\dots\dots\dots\dots\dots\dots\dots\dots\dots\dots \quad (2.52)$$

2.5.2 Minimum Horizontal Stress

The most reliable calculation of minimum horizontal stress can be obtained by hydraulic fracture tests.[52] In such tests increasing the fluid pressure within an isolated part of the wellbore causes a tensile fracture. If we assume that the fluid is keeping the fracture open against the least principal stress, the fluid pressure at which the hydraulic fracture closes is a good estimation of the minimum horizontal stress, S_h. Since the hydraulic fracture tests are not widely undertaken during exploration drilling, leakoff test are being used for estimating the minimum horizontal stress. These tests are routinely performed to determine the maximum mud weight that can be used without generating fractures. The results of leakoff tests are not as reliable as those from hydraulic fracture tests because leakoff is controlled by the disturbed stress field at the borehole wall. But it is accepted that the lower bound of leakoff pressure gives a good and reasonable estimation of minimum horizontal stress.

In the absence of tectonic stresses, it is common to use a linear elastic relationship in which the horizontal stress, S_h, increases with depth as a fraction of the vertical stress[53]:

$$\sigma_h = \left(\frac{\nu}{1-\nu}\right)(\sigma_v - \alpha p_p) + \alpha p_p, \quad \dots\dots\dots\dots\dots\dots\dots\dots\dots\dots\dots\dots\dots\dots \quad (2.53)$$

However, this equation assumes $S_h = S_H$ and no horizontal strain. In addition, it only considers the effects of the overburden stress and pore pressure.

2.5.3 Maximum Horizontal Stress

The maximum horizontal tress, S_H, cannot be determined directly. The best way to constrain its direction and quantity is from observation from image logs, which give

information about the occurrence and orientations of tensile borehole wall fracture and the orientations and widths of breakouts. Then by applying quantitative techniques of wellbore stress analysis, we can constrain the magnitude of S_H[27].

Also the four-arm caliper (dipmeter) can be used to determine the orientation of borehole breakouts. The disadvantage of using this device is that it provides little information about the detailed shape of the borehole and it is not easy to differentiate between key-seats and washouts.

An accurate and proper approach may use observed or calculated values for S_v, p_p, S_h, unconfined strength of rock, the width and position of wellbore failure, and the recorded mud weight used in the well at the depth of the observed failure.

Modeling in deviated wellbores requires first determining the azimuth of maximum horizontal stress consistent with the location of observed borehole breakouts. Afterward, this azimuth will be used to verify and then constrain the magnitude of maximum horizontal stress, using wellbore breakout and drilling-induced tensile fracture observations. Drilling-induced tensile fractures develop just for certain combinations of horizontal stresses and can provide very accurate bounds on maximum horizontal stress magnitudes.[54]

2.5.4 Breakout Angle

Excessive compressional failure of the rock at the borehole wall can cause wellbore collapse. Compressional failure happens when the wellbore stress concentration passes the rock strength and extends from the maximum compressive stress to the point where the stress concentration is just balanced by the rock strength. The angle over which the borehole wall fails in compression mode is known as the breakout width.[27]

In any wellbore stability study, dependent on the situation, we may have different tolerable breakout angles. However, the most common tolerable breakout angle for vertical wells is 90°. We can assume that the critical breakout angle linearly decreases from 90° to 30° if borehole deviation increases from vertical to horizontal.[27]

CHAPTER III
WELLBORE HYDRAULICS

3.1 Background

Calculation of subsurface pressure in gas wells has been studied by many investigators with the results that two widely-used methods have been presented in technical literature. One assumes that temperature and compressibility are constant for the entire gas column. The other assumes that temperature is constant at some average value but permits compressibility to vary with pressure at the constant temperature. These approximations may be justified for shallow and low-pressure wells, but they are unrealistic for deeper, high-pressure wells. In wells experiencing an appreciable change in temperature between the inlet and outlet ends of the flow, it is equally as important to consider the change in compressibility with temperature as it is to consider the change with pressure.

Cullender and Smith[55] developed rigorous equations for calculating subsurface pressures in flowing and static gas wells and pressures along horizontal pipelines. These general equations, based on the mechanical energy balance, contain no assumptions regarding temperature and can be used with any type of temperature gradient (linear or curved). They also recommended a friction factor based on an absolute roughness of 0.0006 in. Flow is always considered to be turbulent.

If we assume that the change in kinetic energy due to the flow of gas is negligible, the general equation for the flow of gas in inclined pipes may be written as follows[55]:

$$\frac{1000 F_s L}{53.33} = \int_{p2}^{p1} \frac{p/ZT \; \mathrm{d}p}{2.6665 \frac{fq^2}{d^5} + \frac{\Delta h}{L} \left(\overline{p/ZT}\right)^2} , \quad \text{..} (3.1)$$

where;

F_s = Specific gravity (Air=1.00),

Δh = Difference in elevation,

L= Length of pipe,

p= Pressure,

q= Rate of flow,

T= Absolute temperature,

Z= Compressibility factor,

d= Internal diameter,

f= Coefficient of friction,

If we let

$$F^2 = \frac{2.6665 \, fq^2}{d^5}, \quad \text{.. (3.2)}$$

then

$$\frac{1000 F_s L}{53.33} = \int_{p2}^{p1} \frac{p/ZT \, dp}{F^2 + \frac{\Delta h}{L}\left(\overline{p}/ZT\right)^2}, \quad \text{.. (3.3)}$$

Without making certain assumptions with respect to *T* and *Z*, mathematical integration of Eq. 3.3 is not possible, but it is possible to solve the integral by using numerical means to evaluate the integral over definite limits.

To evaluate the integration numerically [55]:

$$\int_{p_0}^{p_n} \frac{p/ZT \, dp}{F^2 + \frac{\Delta h}{L}\left(\overline{p}/ZT\right)^2}, \quad \text{... (3.4)}$$

it is necessary to calculate the value of $\left[\dfrac{p/ZT}{F^2 + \dfrac{\Delta h}{L}\left(\overline{p}/ZT\right)^2}\right]$, for p_0 and appropriate

values of p_i where *(i=0, 1, 2, 3…n)*. If we let:

$$I = \frac{p/ZT}{F^2 + \frac{\Delta h}{L}\left(\overline{p}/ZT\right)^2}, \quad \text{.. (3.5)}$$

then

$$\int_{p_0}^{p_n} \frac{p/ZT\, \mathrm{d}p}{F^2 + \frac{\Delta h}{L}\left(\overline{p/ZT}\right)^2} = 1/2\left[(p_1 - p_0)(I_1 + I_0) + (p_2 - p_1)(I_2 + I_1) + \cdots + (p_n - p_{n-1})(I_n + I_{n-1})\right], \quad\cdots\cdots(3.6)$$

In this equation the variation of temperature with length is known, and it is necessary to select appropriate values for the length. After determining the temperature T and p_1 by trial and error we have[55]:

$$37.5\, F_s L_1 = \left[(p_1 - p_0)(I_1 + I_0) + (p_2 - p_1)(I_2 + I_1)\right], \quad\cdots\cdots (3.7)$$

$$37.5\, F_s L_2 = \left[(p_1 - p_0)(I_1 + I_0) + (p_2 - p_1)(I_2 + I_1) + (p_3 - p_2)(I_3 + I_2)\right], \quad\cdots\cdots (3.8)$$

$$\vdots$$

$$37.5\, F_s L = \left[(p_1 - p_0)(I_1 + I_0) + (p_2 - p_1)(I_2 + I_1) + \cdots + (p_n - p_{n-1})(I_n + I_{n-1})\right], \quad (3.9)$$

This method can be tedious if a large number of increments are chosen for L; however, by means of a two-step calculation and the application of Simpson's[56] rule, reasonable accuracy can be obtained.

3.2 Flow Equations

3.2.1 The Horizontal Flow Equation

For horizontal flow, $\Delta h = 0$, and Eq. 3.3 becomes:

$$\frac{1000 F_s L F^2}{53.33} = \int_{p2}^{p1} p/ZT\, \mathrm{d}p, \quad\cdots\cdots (3.10)$$

and Eq. 3.9 becomes:

$$37.5\, F_s L F^2 = \left[(p_1 - p_0)(I_1 + I_0) + (p_2 - p_1)(I_2 + I_1) + \cdots + (p_n - p_{n-1})(I_n + I_{n-1})\right], \quad (3.11)$$

where

$$I = p/ZT, \quad\cdots\cdots (3.12)$$

3.2.2 Inclined Static Column

For a static column of gas $q=0$, therefore $F^2=0$, then Eq. 3.3 can be shown as follows:

$$\frac{F_s \Delta h}{53.33} = \int_{p_c}^{p_f} ZT/p\, \mathrm{d}p, \quad\cdots\cdots (3.13)$$

where;

p_c= Shut-in wellhead pressure,

p_f = Formation Pressure,

And Eq. 3.9 becomes:

$$0.0375\,F_s\Delta h = \left[(p_1 - p_0)(I_1 + I_0) + (p_2 - p_1)(I_2 + I_1) + \cdots + (p_n - p_{n-1})(I_n + I_{n-1})\right], \quad (3.14)$$

where

$$I = ZT/p, \quad\dots\dots\dots\dots\dots\dots\dots\dots\dots\dots\dots\dots\dots\dots\dots\dots\dots\dots\dots\dots\dots\dots\dots\dots \quad (3.15)$$

3.2.3 Positive Inclined Flow Equation (Production in a Gas Well)

For upward inclined flow, Eq. 3.3 becomes:

$$\frac{1000 F_s \Delta h}{53.33} = \int_{p_W}^{p_S} \frac{p/ZT\ \mathrm{d}p}{\dfrac{L}{\Delta h}F^2 + \left(\overline{p}/ZT\right)^2}, \quad\dots\dots\dots\dots\dots\dots\dots\dots\dots\dots\dots\dots\dots\dots\dots \quad (3.16)$$

where;

p_w= Flowing wellhead pressure,

p_s= Flowing sandface pressure,

and Eq. 3.9 becomes:

$$37.5\,F_s\Delta h = \left[(P_1 - P_0)(I_1 + I_0) + (P_2 - P_1)(I_2 + I_1) + \cdots + (P_n - P_{n-1})(I_n + I_{n-1})\right], \quad .(3.17)$$

where,

$$I = \frac{p/ZT}{\dfrac{L}{\Delta h}F^2 + \left(\overline{p}/ZT\right)^2}, \quad\dots\dots\dots\dots\dots\dots\dots\dots\dots\dots\dots\dots\dots\dots\dots\dots\dots\dots \quad (3.18)$$

3.2.4 Negative Inclined Flow Equation (Gas Injection in a Well)

For downward inclined flow, Eq. 3.3 becomes:

$$\frac{1000 F_s \Delta h}{53.33} = \int_{p_W}^{p_S} \frac{p/ZT \ dp}{-\dfrac{L}{\Delta h} F^2 + \left(\overline{p/ZT}\right)^2} \ , \quad \text{..} \quad (3.19)$$

$$37.5 \ F_s \Delta h = \left[(p_1 - p_0)(I_1 + I_0) + (p_2 - p_1)(I_2 + I_1) + \cdots + (p_n - p_{n-1})(I_n + I_{n-1}) \right], \quad (3.20)$$

where

$$I = \frac{p/ZT}{-\dfrac{L}{\Delta h} F^2 + \left(\overline{p/ZT}\right)^2} \ , \quad \text{..} \quad (3.21)$$

3.3 Coefficient of Friction

To determine the term I in different flow equations, we have to evaluate the term F^2 in Eq. 3.2. Evaluation of F^2 depends on the appropriate selection of coefficient of friction f and diameter d. Because the diameter is known for any specific case, the coefficient of friction f should be determined for the particular case. Coefficient of friction f may be obtained from different correlations; however, in this research, fluid flow in the wellbore can be considered as "completely rough flow" portion of Moody's[57] curves. Moody's curves were calculated based on Colebrook's[58] equation.

The Colebrook equation, developed in 1938, states that for Reynolds numbers greater than 3,000, a pipe's coefficient of friction, f, is a function of both Reynolds number and relative roughness. Relative roughness is:

$$\varepsilon_D = \frac{\varepsilon}{d}, \quad \text{..} \quad (3.22)$$

where;

ε = Absolute roughness,

ε_D = Relative roughness,

The implicit form of Colebrook equation can be stated as below:

$$\frac{1}{\sqrt{f}} = -2\log_{10}\left(\frac{\varepsilon_D}{3.7} + \frac{2.51}{N_{Re}\sqrt{f}}\right), \quad \text{...} \quad (3.23)$$

where N_{Re} is Reynolds number.

These equations can be solved for f given the relative roughness ε_D and the Reynolds number, N_{Re}, by iteration.

CHAPTER IV

FIELD CASE INVESTIGATION

4.1 Background

The consulting engineering firm John Wright Company (JWCO) provided the field data[59] for our blowout self-killing investigation. Available data include the blowout scenario prior to bridging (**Fig. 4.1**[59]) and noise and temperature logs along the wellbore (**Fig. 4.2**[59]). Gamma-ray logs in that report indicate some bridging behind the pipe from around 1000 m true vertical depth (TVD) to the top of the first gas sands at around 2200 m TVD, and also another plug within the depth of 2670 to 2680 m TVD.

The blowout well (SWA-184 ST1) was the first sidetrack from a production well. The operator cut a window at 490 m TVD and drilled a 12 ¼-in. hole from the window to the current true depth (TD) of the well, which is 3068 m measured depth (MD) and 2800 m TVD (**Fig. 4.3**)[59]. Wellbore trajectory includes a build-and-hold section with kick-off point at 490 m TVD. Inclination angle is 26.3°, and wellbore azimuth is -293°.
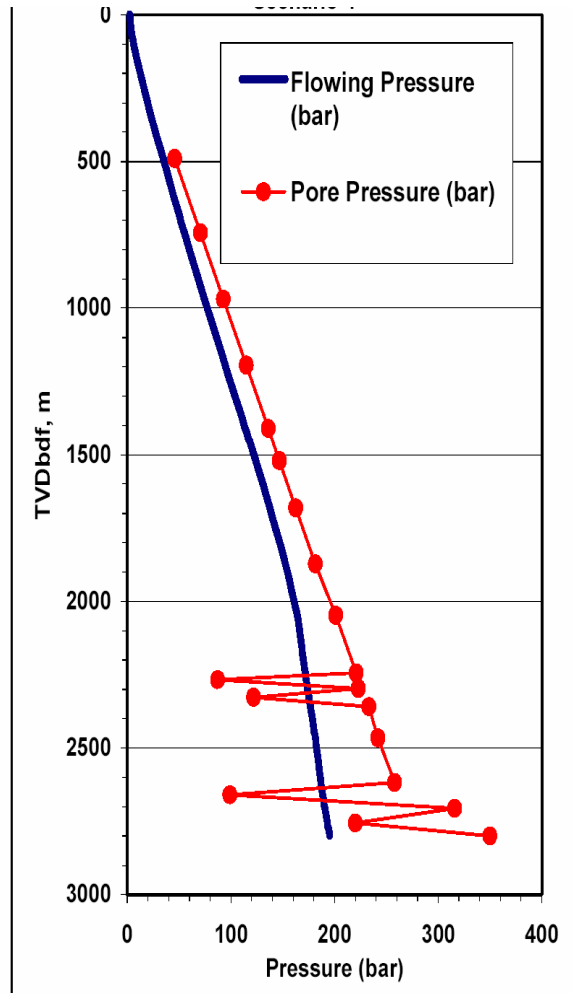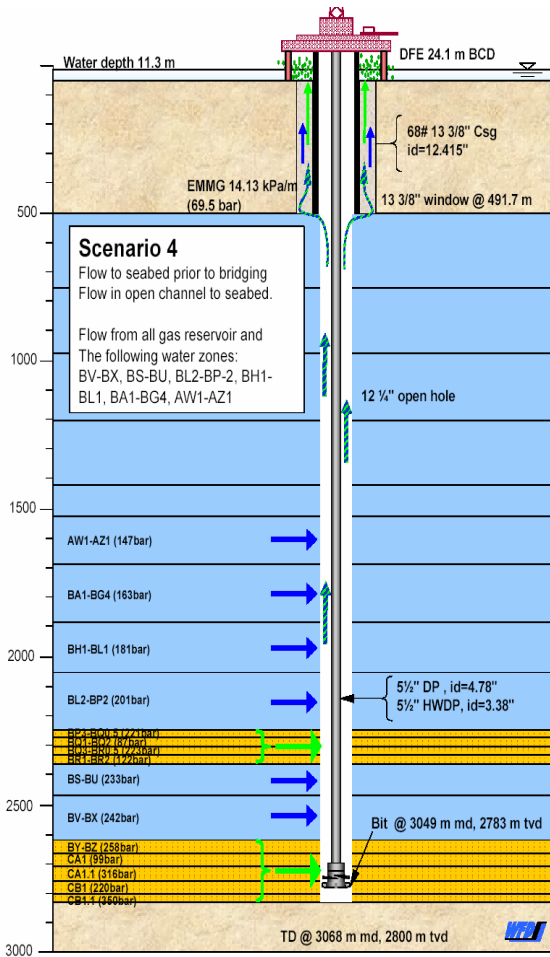
Fig. 4.1—Scenario 4, Sketch of scenario definition and simulated flowing bottomhole pressure (from Wright[59]).
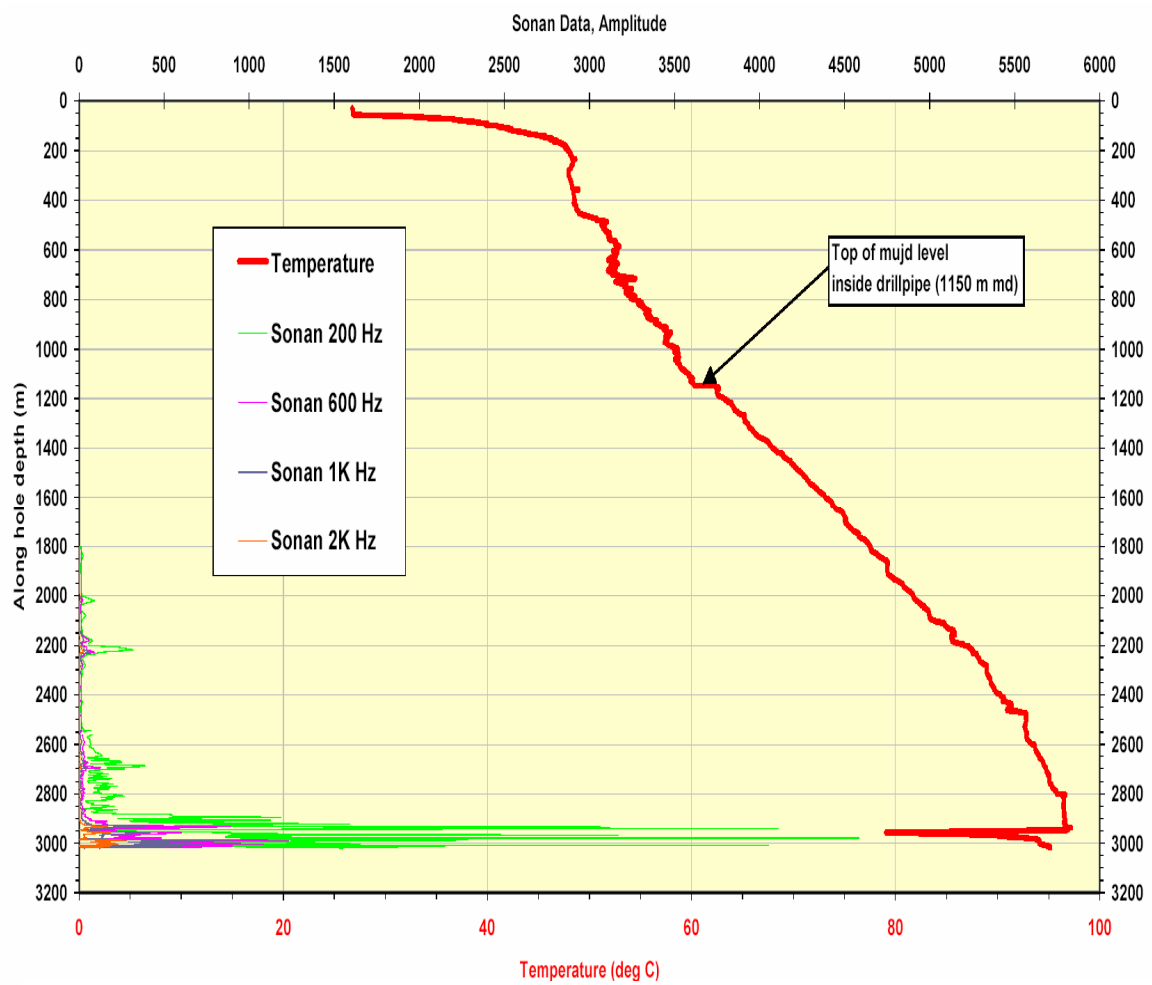
Fig. 4.2—Temperature and noise log along hole depth (fromWright[59]).
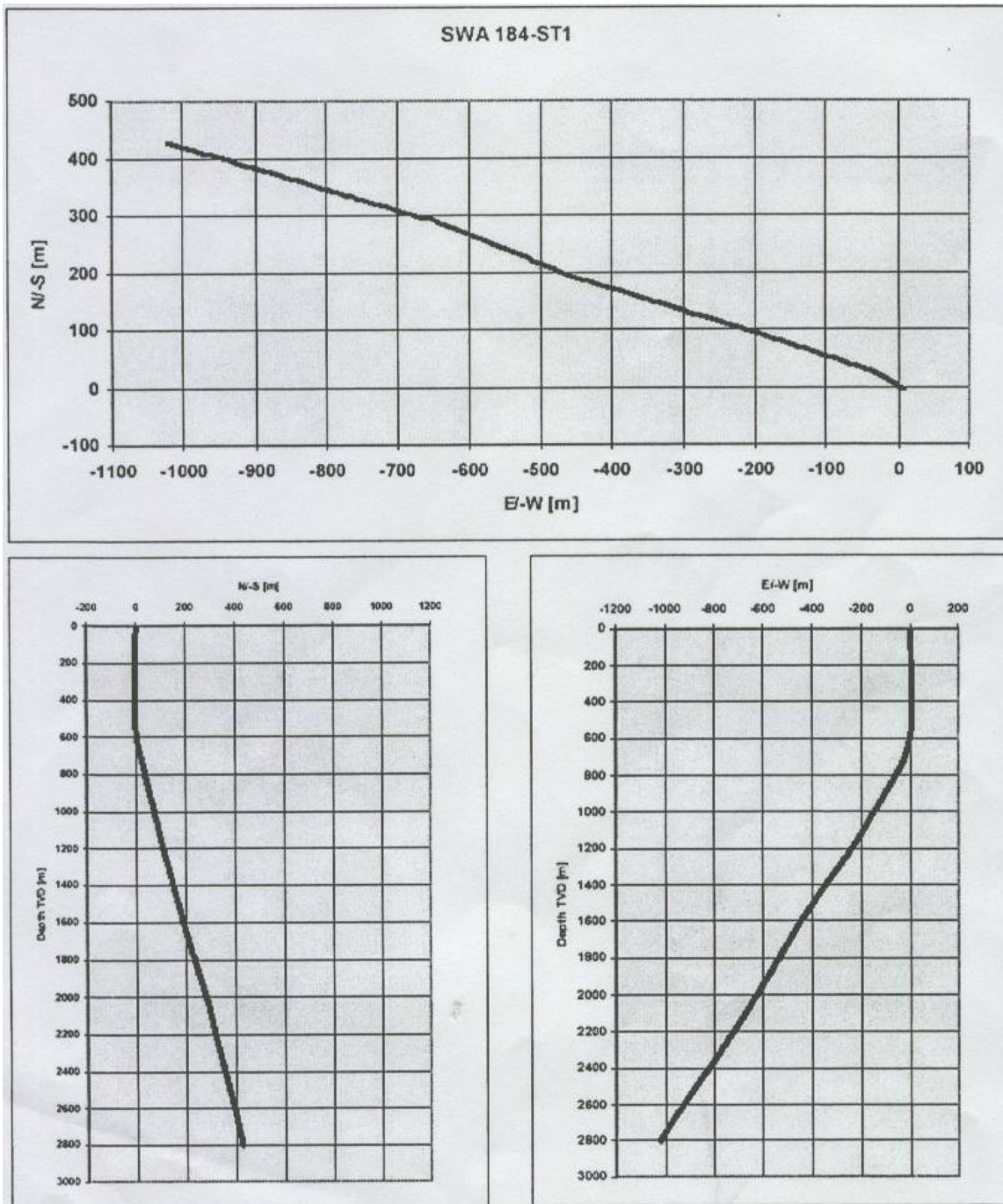
Fig. 4.3—Trajectory of Well SWA 184-ST1 (from Wright[59]).

The well took a gas kick at 2,800 m TVD. After trying to circulate out the kick, the operator observed gas leakage around the casing and gas broaching to the surface underneath the platform.

JWCO used the OLGA2000 simulator to investigate and simulate the blowout. They used the reservoir inflow performance curve as the inlet condition and selected seabed conditions as the other boundary condition in the system or fracturing pressure at the shoe (491 m TVD) for some of the cases.

The observations showed a good washout from the casing shoe up to the surface. Therefore, the scenario with open flow path was selected as most realistic scenario (**Fig. 4.1**). This scenario assumes that the system has too low restrictions to make any significant back pressure from the casing shoe up to the seabed.

4.2 Simulation of Wellbore Bridging

4.2.1 Geomechanical Model

Generally, a geomechanical model consists of the magnitude and orientation of the three principal stresses, the pore pressure, and the uniaxial compressive rock strength.

In our approach to analyze the wellbore bridging, we constructed a geomechanical model suitable for our case with four main subroutines we developed. The first one is related to the in-situ field stresses acting in the wellbore region. The second subroutine is a computational module that calculates the fluid pressure profile along the welbore. (The other alternative for this subroutine is the fluid pressure profile obtained from observations or any other fluid flow simulator.) The third subroutine has been designed to determine the formation properties from sonic interval transient time, and the fourth subroutine has been created to integrate the previous three modules into a bridging simulation. As input data in calculations, we have used well-specific data such as TVD, pore pressure, inclination, and angle between maximum horizontal stress and wellbore direction.

4.2.2 In-Situ Field Stresses

In deviated wells it is not possible to determine the direction of the maximum horizontal stress directly from the geographic azimuth of observed failures, and further modeling is required. However, in our case, in-situ field stresses were calculated from published data about Brunei field stresses. This region has a normal stress regime with maximum vertical stress and a high level of anisotropy throughout the field, with the maximum horizontal stress oriented on the 314° direction. Therefore, the angle between the wellbore and maximum stress direction is 21°. In-situ stress orientation in the field is shown in **Fig. 4.4**.[59]
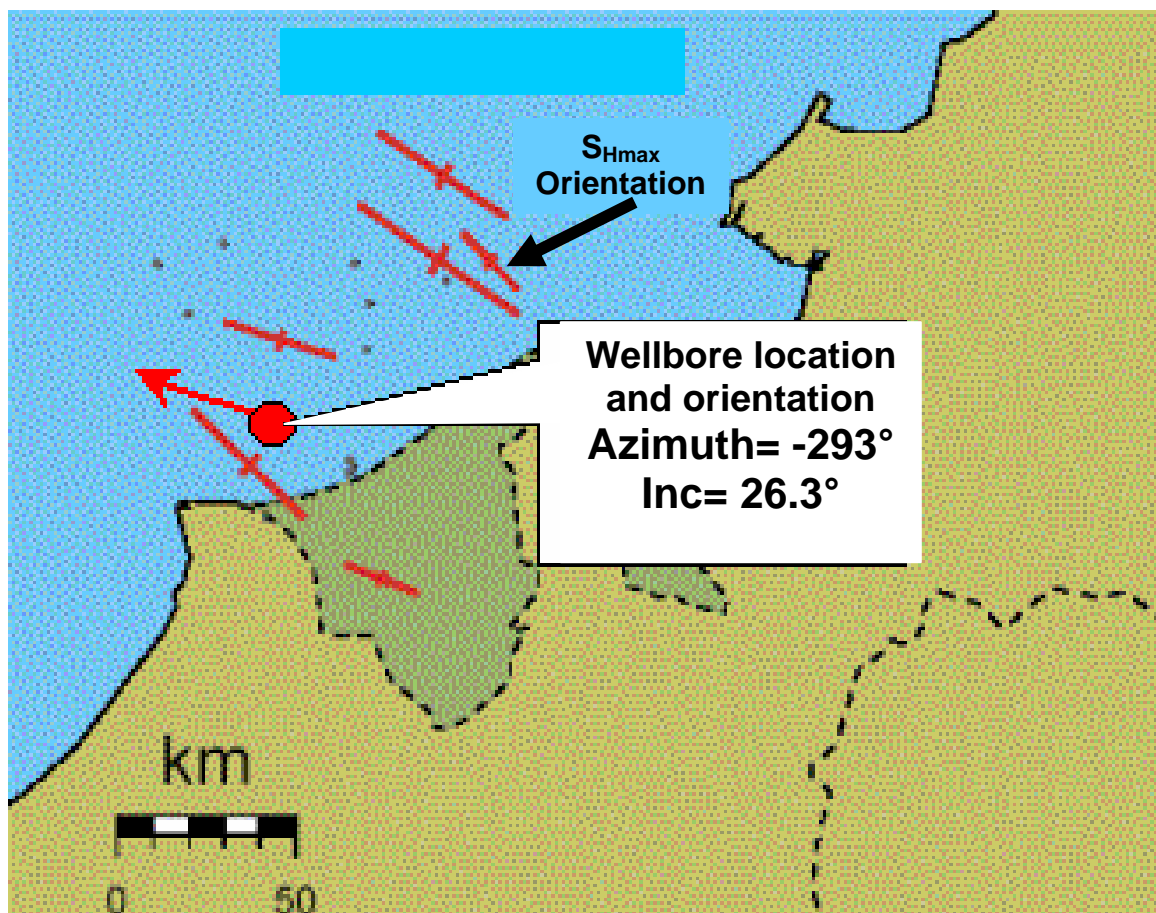

Fig. 4.4—In-situ stress orientation and wellbore location (from Wright[59]).

The vertical stress gradient changes between 0.8 and 1.05 psi/ft. For minimum horizontal stress, we used a correlation developed by Breckels and Eekelen[60] from 15 hydraulic fracturing tests for this production field. All of these data were from minifracture tests carried out specifically to determine stress levels, rather than from large-scale stimulation treatments. After the pore pressure adjustment, they came up with full relationship for Brunei region shown by Eq. 4.1:

$$S_h = 0.227\, z^{1.145} + 0.49\left(p_p - p_{pn}\right),$$ .... (4.1)

where;

z = True vertical depth,

P_{pn} = Normal pore pressure,

This correlation is valid for depths of 0 to 10,000 ft.

Usually, after the azimuth of the maximum horizontal stress is determined, we can use the azimuth to verify and then constrain the magnitude of maximum horizontal stress using both borehole breakout and drilling-induced tensile fracture observations. However, in our study because of the high stress anisotropy, we assumed that the magnitude of maximum horizontal stress is equal to vertical stress.

4.2.3 Rock Mechanical Properties

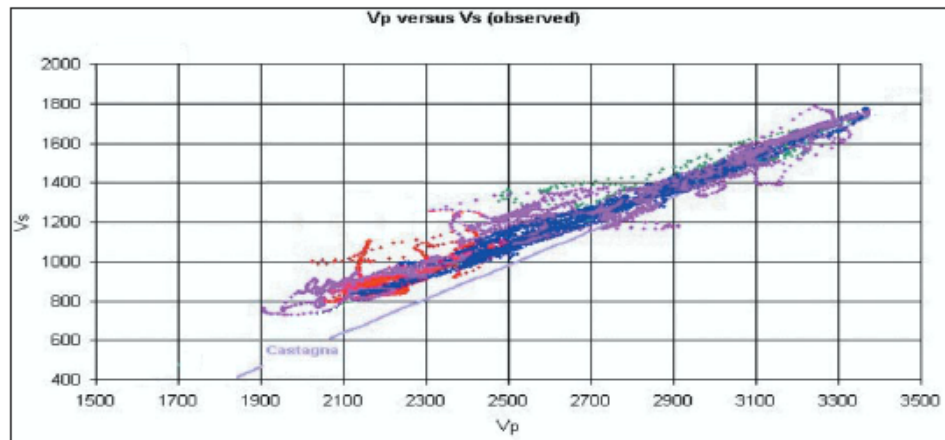We have used sonic logs typical for the region of interest to obtain formation properties (**Fig 4.5** and **Fig. 4.6**).[61]

Fig. 4.5—Crossplot of V_p and V_s (from Lindsay and Foster[61]).
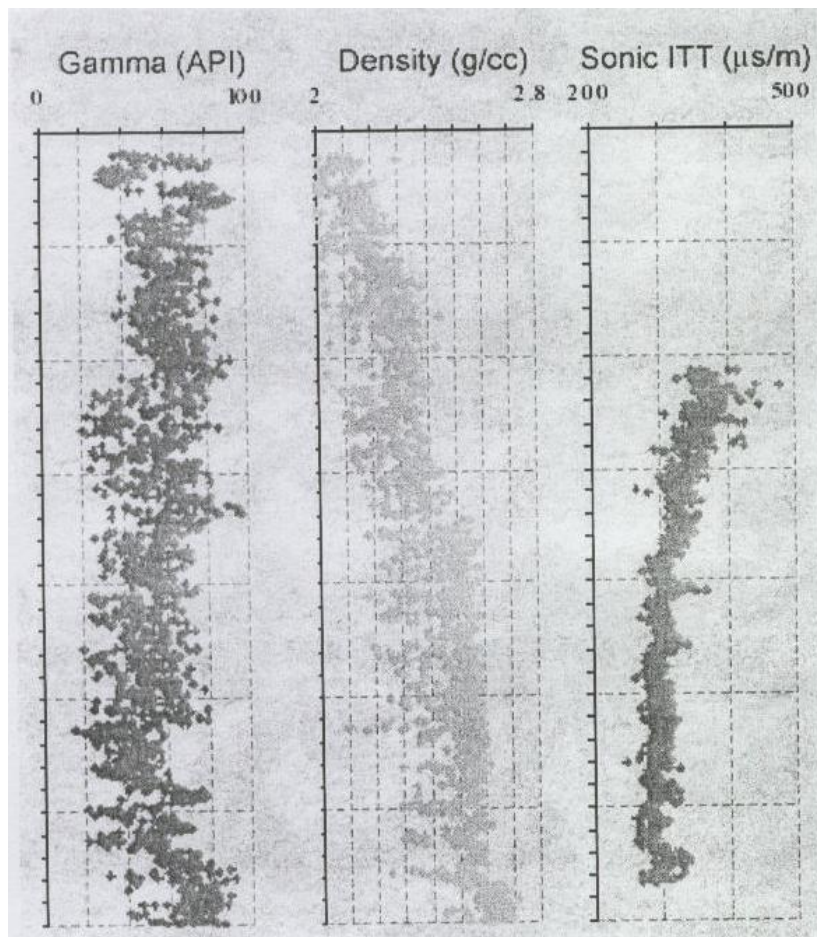

Fig. 4.6—Logs used to obtain the strength properties of shale (from Wright[59]).

Having the compressional sonic velocity, we obtained the angle of internal friction ϕ_f, and cohesion S_0 (**Fig. 4.7**), from Manohar's[51]shale strength correlation. These relations (Eq. 2.51 and Eq. 2.52) were developed from extensive shale database.
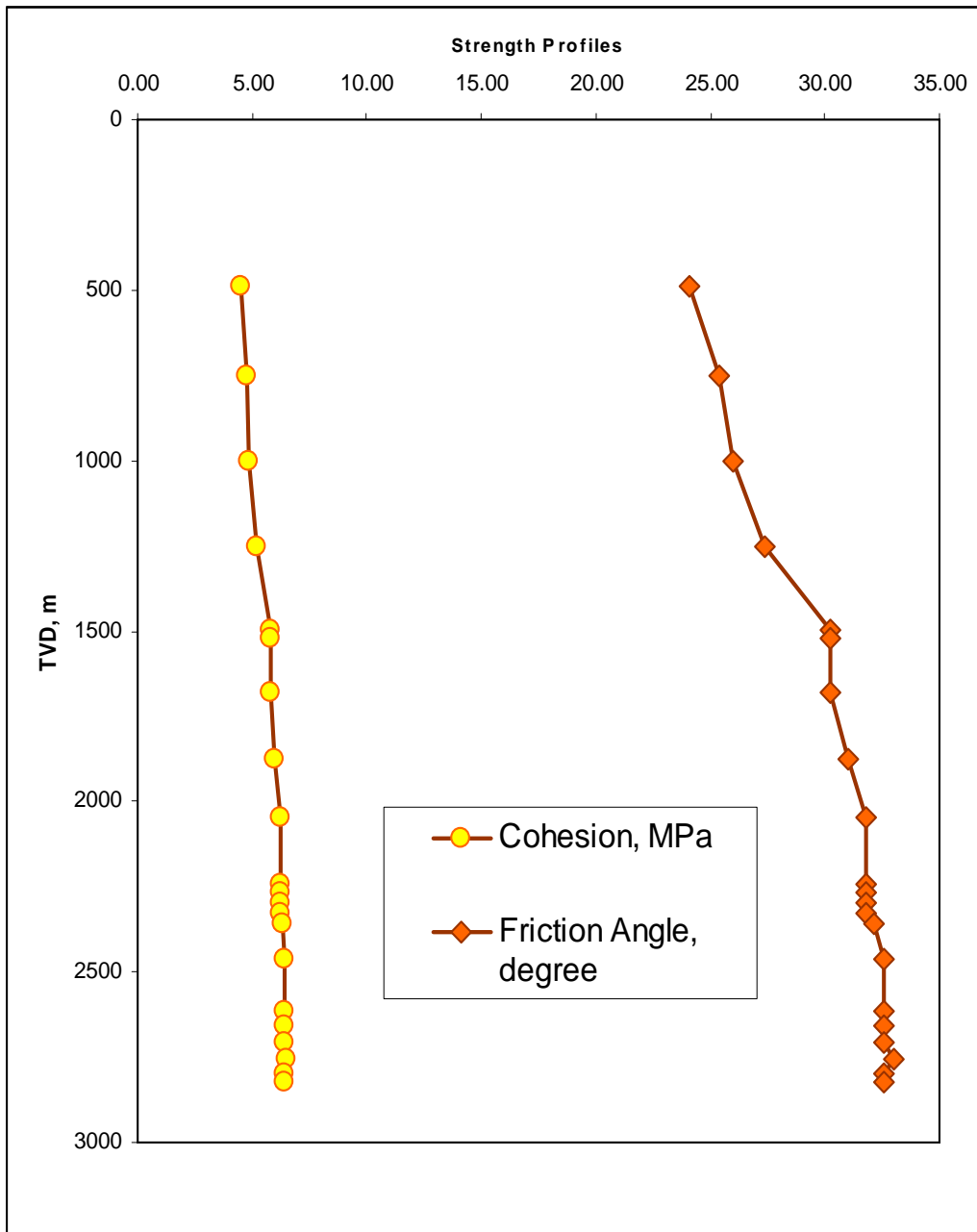

Fig. 4.7—Cohesion and internal friction angle calculated for field of interest.

4.2.4 Failure Criteria

4.2.4.1 Shale Intervals

For shale intervals we used the Mohr-Coulomb and Modified-Lade criteria to compare the results of these two different approaches.

4.2.4.2 Universal Strength Correlation for Sandstones

For sandstones we used Zhang *et al.*'s[62] universal correlation and strength criteria as a function of compressional sonic velocity V_p (kft/sec), and critical pressure p_{crit} (kpsi) as below:

$$\overline{P}_e = \frac{(\sigma_1 + \sigma_2 + \sigma_3)}{3} - \alpha p_p , \quad \text{...} \quad (4.2)$$

$$\Delta \sigma = \sqrt{\frac{1}{2}\left[(\sigma_1 - \sigma_2)^2 + (\sigma_1 - \sigma_3)^2 + (\sigma_2 - \sigma_3)^2\right]}, \quad \text{.................................} \quad (4.3)$$

where;

P_e = Mean effective pressure,

$\Delta \sigma$ = Differential stress,

According to Eq. 2.2 and the fact that our interest area of study is porous sandstone, the matrix compressibility is much smaller than bulk compressibility, so we can assume that $\alpha = 1$.

In their study, they performed a series of laboratory tests for sandstone samples to develop an approach to evaluate formation strength. They developed an efficient correlation between the critical pressure and the in-situ compressional velocity.

Next, they calculated the critical pressure as below:

$$p_{crit} = 10.086 \ln \frac{6.789}{12.322 - V_p} , \quad \text{..} \quad (4.4)$$

Finally, after normalizing all strength data by the corresponding critical pressures, all data converged to a single curve having the form:

$$y = \alpha_0 + \alpha_1 x + \alpha_2 x^2 + \alpha_3 x^3 , \quad x \neq 1 , \quad \text{..........................} \quad (4.5)$$

or

$$0 \le y \le 0.243, \quad x = 1, \quad \text{...} \quad (4.6)$$

where

$$y = \frac{\Delta\sigma}{p_{crit}}, \quad \text{...} \quad (4.7)$$

and

$$x = \frac{\overline{p_e}}{p_{crit}}, \quad \text{...} \quad (4.8)$$

In these equations, $\alpha_0 = 0.019$, $\alpha_1 = 1.795$, $\alpha_2 = -1.540$, and $\alpha_3 = -0.03$.

For any normalized deviated stress ($\frac{\Delta\sigma}{p_{crit}}$) above the envelope curve, the wellbore wall

will fail.

4.2.5 Pore Pressure and Wellbore Pressure

The wellbore pressure profile and pore pressure profile were obtained from the report
JWCO provided, presented in **Fig. 4.1**.

4.3 Bridging Simulation

Using Mohr-Coulomb, Modified-Lade, and strength correlations for sandstones criteria,
we compared induced stresses in the vicinity of the wellbore with rock strength to
determine the potential locations of fractured or collapsed intervals. We used an elastic
model using a three-dimensional generalized plane-strain solution to compare the
induced stresses and rock strength. All three failure criteria in our model use the input
strength parameters presented in **Fig. 4.7**. Three cases were simulated with different
wellbore pressure profiles to try to match the bridging. Because it is a deviated well, we
considered the critical angle as 120° and considered any location with breakout angle
greater than this critical value as a potential part for wellbore failure or bridging.

4.3.1 Normal Drilling Operation

We ran the simulation for the openhole section with mud weights used before blowout (10.1 lb/gal). Simulation results for Modified-Lade and Mohr-Coulomb criteria are presented in **Fig.4.8** and **Fig.4.9**.
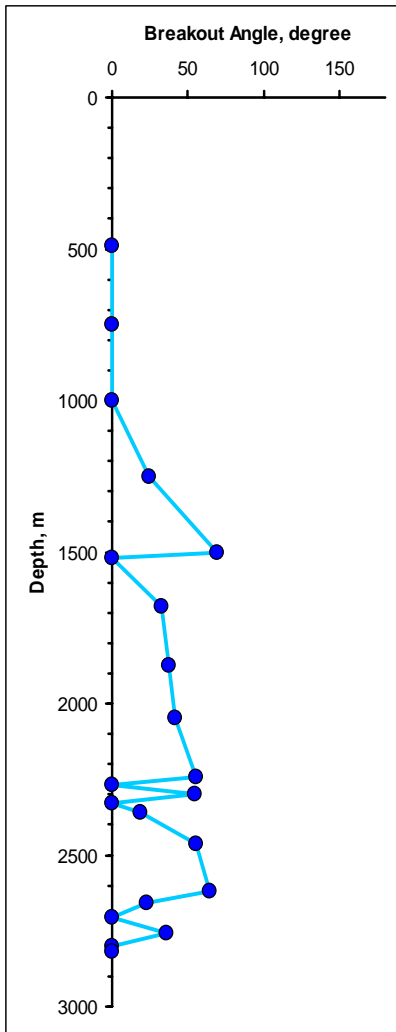

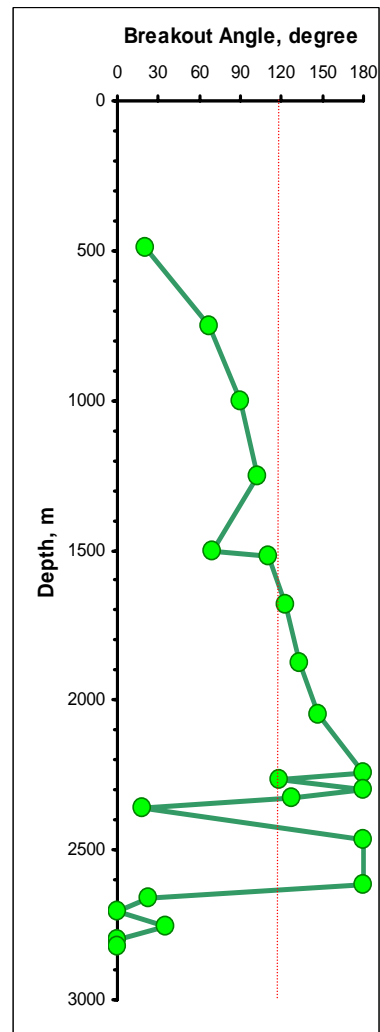**Fig. 4.8**—Breakout angles for normal operation based on Modified-Lade criteria .

Fig. 4.9—Breakout angles for normal operation based on Mohr-Coulomb criteria.

Modified-Lade simulation results demonstrate that before blowout the borehole was

stable along its total length, while Mohr-Coulomb simulation results show wellbore failure around 1681 m to 2620 m.

4.3.2 Blowout Situation

As a second set of the simulation pressure values along the wellbore was obtained from the most probable reported blowout scenario. We used the modeled wellbore pressure to predict massive wellbore collapse. **Fig. 4.10** shows the results of the simulation.
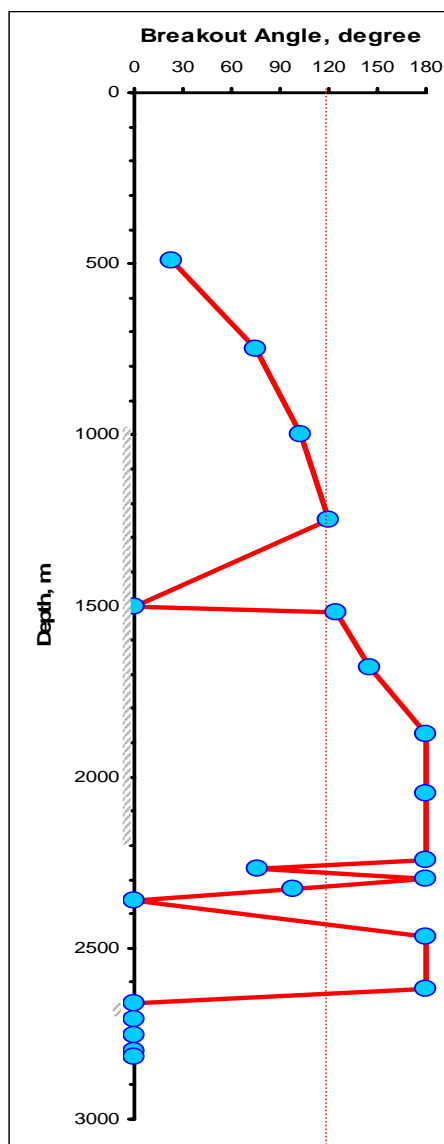

Fig. 4.10—Blowout: Wellbore pressure from OLGA2000.

In this simulation we applied the Modified-Lade failure criterion for borehole failure determination. Simulation results demonstrate that borehole collapse is likely to occur within the depth ranges of 1520 to 2240 m, 2280 to 2325 m and 2475 to 2626 m.

      Fig. 4.11 shows the results for the third set of simulations. In this simulation we used the wellbore pressure profile obtained from our simulator.
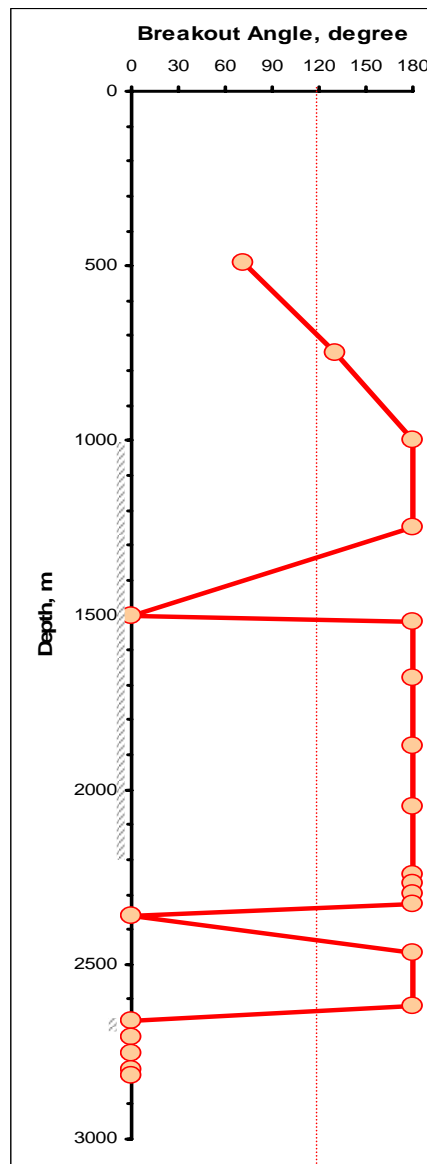

Fig. 4.11—Blowout, modified-Lade: Wellbore pressure from our simulator.

According to the most probable scenario for our case, which assumes open flow path, there is not enough restriction to make any significant back pressure. Therefore, for simulating the wellbore pressure during blowout we modeled the flow of gas only, which is consistent with the blowout scenario, but with the observed gas flow rate of 150,000 Mscf/D. In this case the bridging is expected within the depth range of 700 to 1340 m, 1525 to 2340 m and 2475 to 2625 m.

To compare the results, we simulated with the Mohr-Coulomb criteria as well. **Fig. 4.12** shows the results.
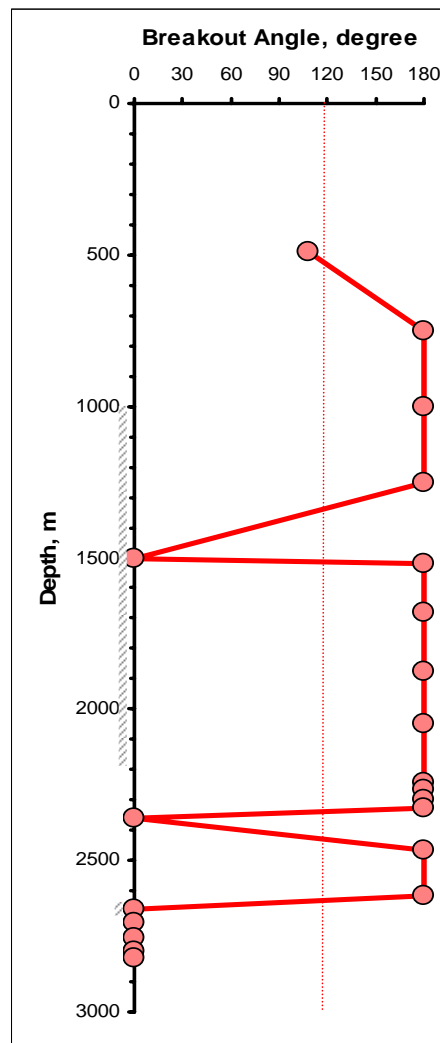

Fig. 4.12— Blowout, Mohr-Coulomb: Wellbore pressure from our simulator.

According to the Mohr-Coulomb criterion and based on the wellbore pressure profile obtained from our simulator, bridging is expected within the depths of 530 to1340 m, 1525 to 2340 m and 2475 to 2625 m.

Results from both simulations, i.e. the one based on the pressure profile obtained from OLGA2000 and the one which used our modeled gas flow along the wellbore, demonstrate almost the same results. According to these simulations, bridging is most expected within shale formations. The reason is that the magnitude of in-situ stresses increases while the strength of the shale does not change significantly.

To check the accuracy of our simulator, we applied GMI's Stress and Failure of Inclined Boreholes (GMI•SFIB) software for normal drilling operations. This software provides fully 3D stress modeling for both wellbore breakouts and tensile wall fractures. **Fig. 4.13** shows the SFIB's result for TVD of 2327 m.
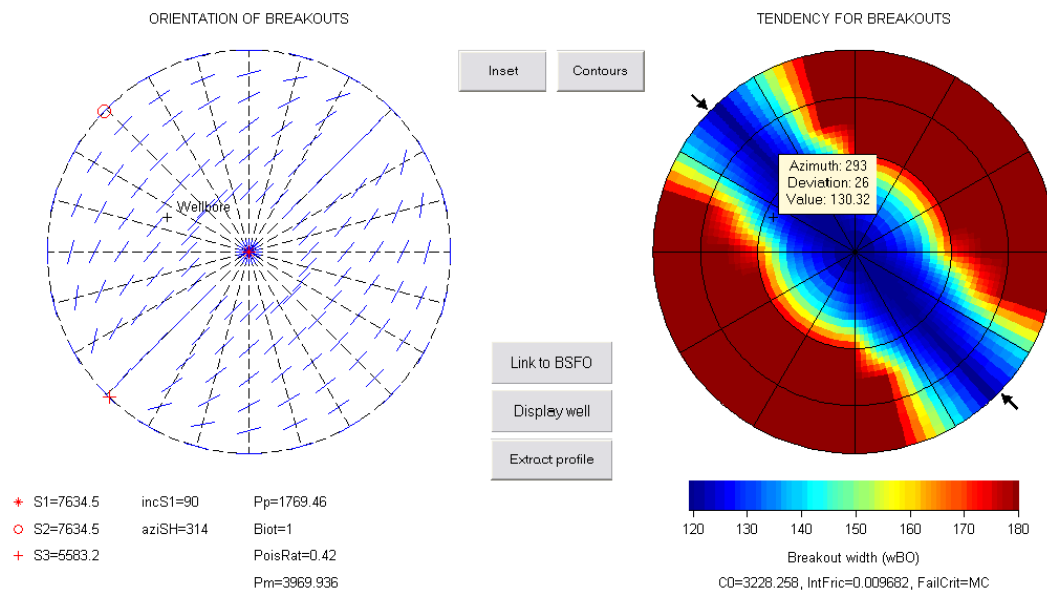

Fig. 4.13—Breakout angle at TVD=2327 m.

Fig. 4.14 compares the breakout angle values along the wellbore for our simulator and SFIB software based on Mohr-Coulomb failure criterion.
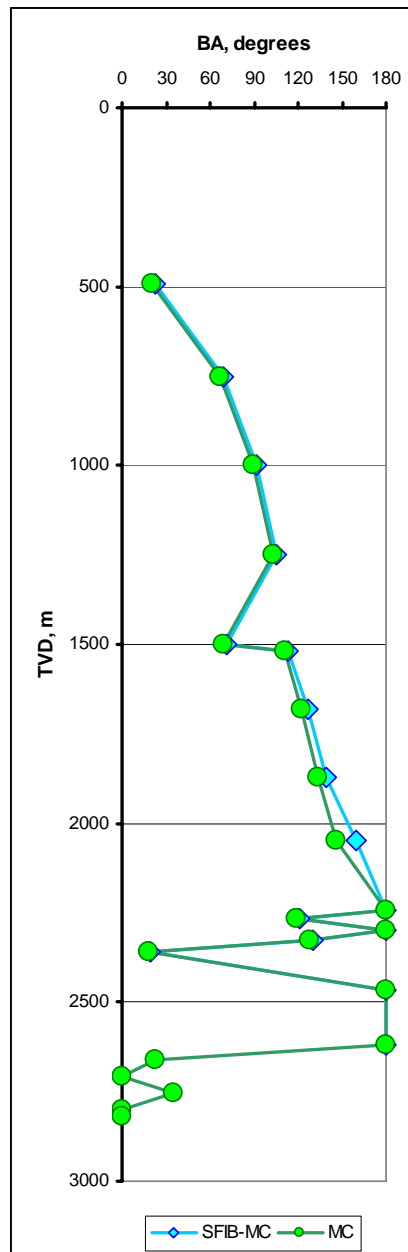

Fig. 4.14—Comparison of SFIB and our simulator for normal operation.

This comparison demonstrates good match between our simulator and SFIB software.

Fig. 4.15 shows the comparison between Mohr-Coulomb and modified-Lade criteria for normal drilling operations.
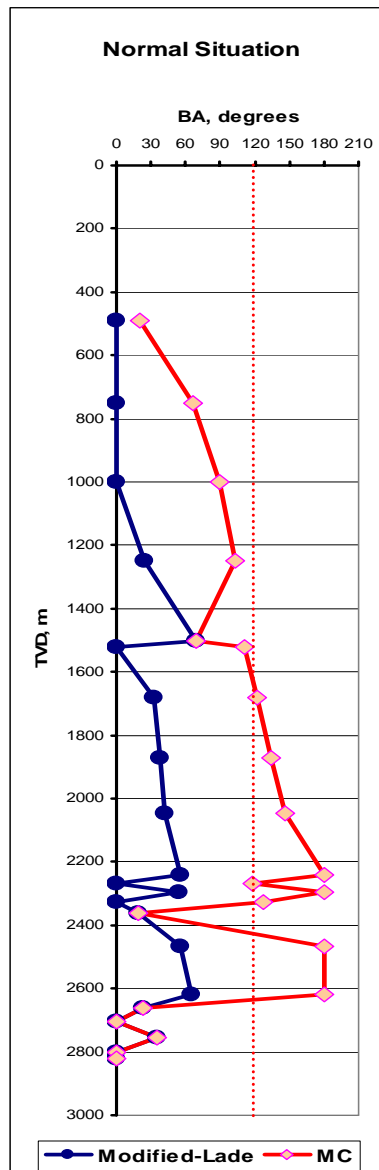

Fig. 4.15—Mohr-Coulomb and modified-Lade for normal situations.

Fig. 4.16 shows the comparison of three simulations for the pressure profile obtained from OLGA2000 and our gas flow model.
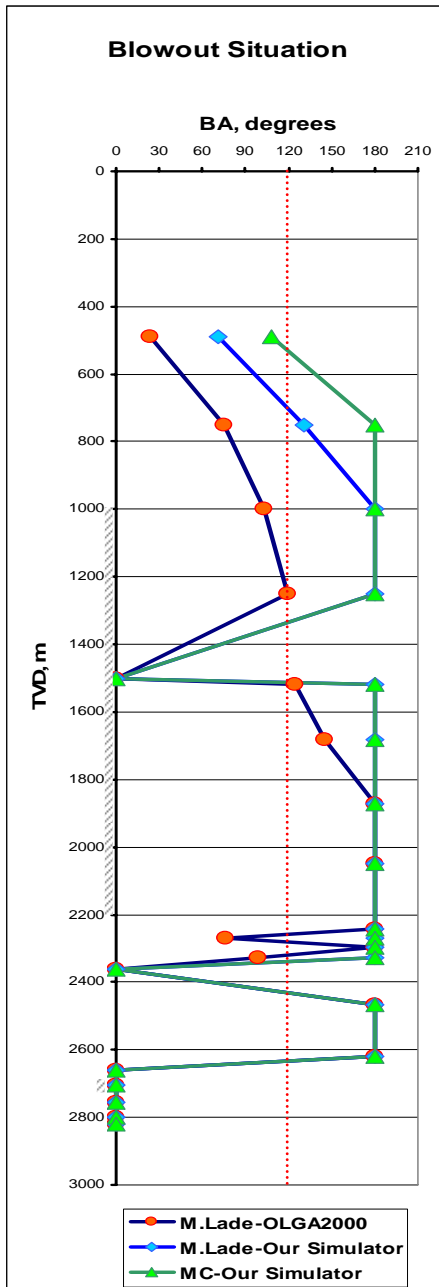

Fig. 4.16—Comparison of three sets of simulation.

CHAPTER V
DEEPWATER GOM

5.1 Water Depth Effect

Having validated the performance of our simulator with the Brunei's case study, we used our simulator to study the probability of wellbore bridging during blowouts in deepwater GOM. Since we could not find real data in deepwater GOM that could be used in our study, we used general trends and most probable values for this study. Some assumptions we have taken in this approach are:

- Wellbore geometry= vertical.
- Wellbore diameter = 7 7/8 in.
- Formation = shale.
- No mud in wellbore during blowout.
- Open flow path during blowout (no back pressure).
- Fixed outlet pressure= hydrostatic pressure at seabed.
- Gas gravity (air=1) = 0.65.

5.2 In-Situ Field Stresses

5.2.1 Overburden Stress

In normal practices it is quite common to assume overburden gradient 1 psi/ft. However, this is a high average value for a nonconstant variable, and it can be seriously in error in some areas, like the gulf coast at shallow depths.[63] According to Eaton[63], in the gulf coast area the average overburden stress gradient does not equal 1 psi/ft; instead it is about 0.85 psi/ft near the surface and increases smoothly to 1 psi/ft at about 20,000 ft of depth.

To apply the effect of different overburden gradients for different depths in our study, we used Eaton's[63] overburden stress gradient for normally compacted gulf coast formations (**Fig. 5.1**).
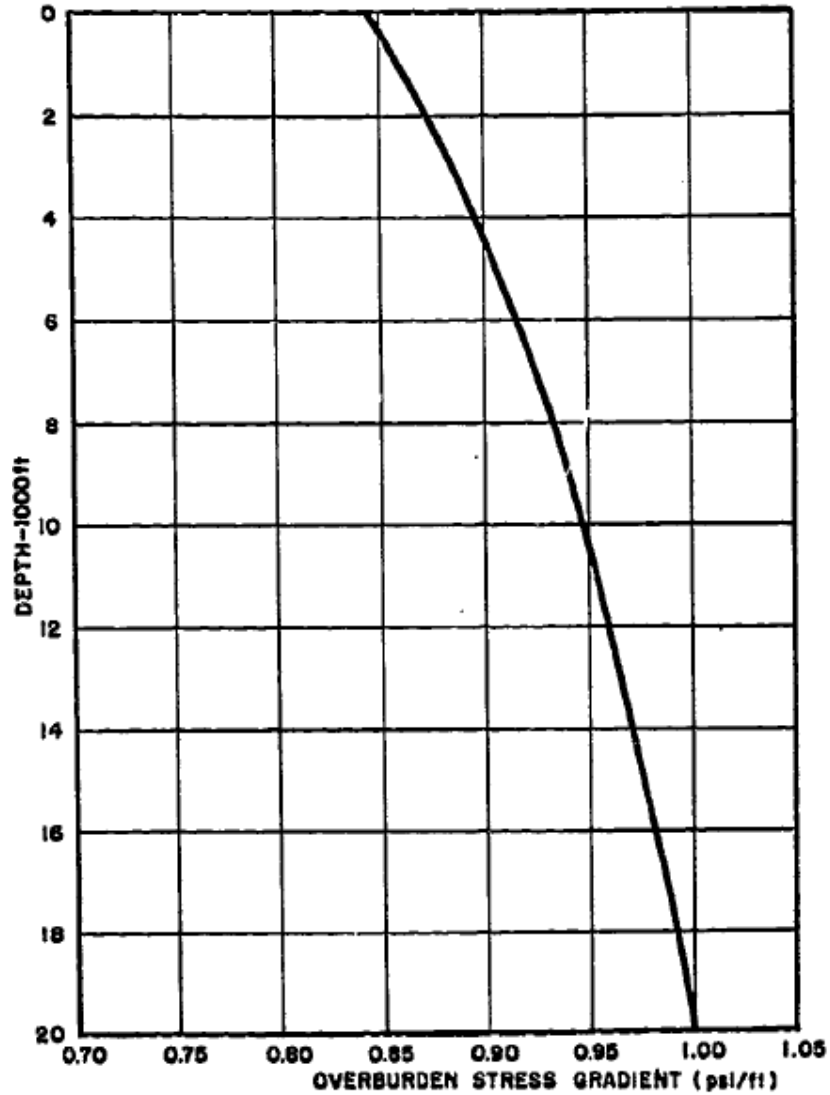
55

Fig. 5.1—Composite overburden stress gradient for all normally
compacted Gulf Coast formations(from Eaton[63]).

For any specific depth, the corresponding overburden stress gradient is the real
average overburden gradient at that depth. However, the curve in **Fig. 5.1** is not for
offshore applications, and hydrostatic pressure of water is not considered. Therefore, in
our case for any depth below the mudline the maximum vertical stress is the summation

of overburden gradient from **Fig. 5.1** multiplied by the depth and hydrostatic pressure of sea water.

5.2.2 Maximum Horizontal Stress

Since we could not find any correlation for maximum horizontal stress for deepwater GOM, we assumed three different assumptions for calculating maximum horizontal stress.

First we assumed that for any depth the maximum horizontal stress is equal to the maximum vertical stress at that depth. This is a good assumption for areas characterized by normal faulting systems.

The second assumption is based on the strike-slip faulting system condition. To calculate the maximum horizontal stress in this condition, we used Anderson's faulting theory[64]:

$$\frac{\sigma 1}{\sigma 3} = \frac{S_H - p_p}{S_h - p_p} \leq \left[\left(\mu_f^2 + 1 \right)^{\frac{1}{2}} + \mu_f \right]^2 , \quad \text{...............................} (5.1)$$

According to the laboratory tests, a coefficient of friction of 0.6 to 1 is applicable in any faulting system. If we assume a coefficient of friction equal to 0.6, for the case of frictional equilibrium we can rewrite the above equation as:

$$S_H = 3.1 \times S_h - 2.1 \times p_p , \quad \text{...} (5.2)$$

Finally, in the third case we assumed that the maximum horizontal stress is equal to the minimum horizontal stress.

5.2.3 Minimum Horizontal Stress

We used generic data from deepwater GOM to obtain the fracture gradients for different seawater depths. Then we assumed that for any specific depth below mudline, the minimum horizontal stress is equal to depth multiplied by the fracture gradient at that depth.

5.3 Rock Mechanical Properties

5.3.1 Angle of Internal Friction and Cohesion

To obtain the angle of internal friction, ϕ_f, and cohesion, S_0, of shale, Gardner's[65] general sand/shale velocity relationship for the GOM under normal pressure conditions has been used. **Fig. 5.2**[65] shows the general trend for normally pressured Miocene sandstone and shale in the GOM.
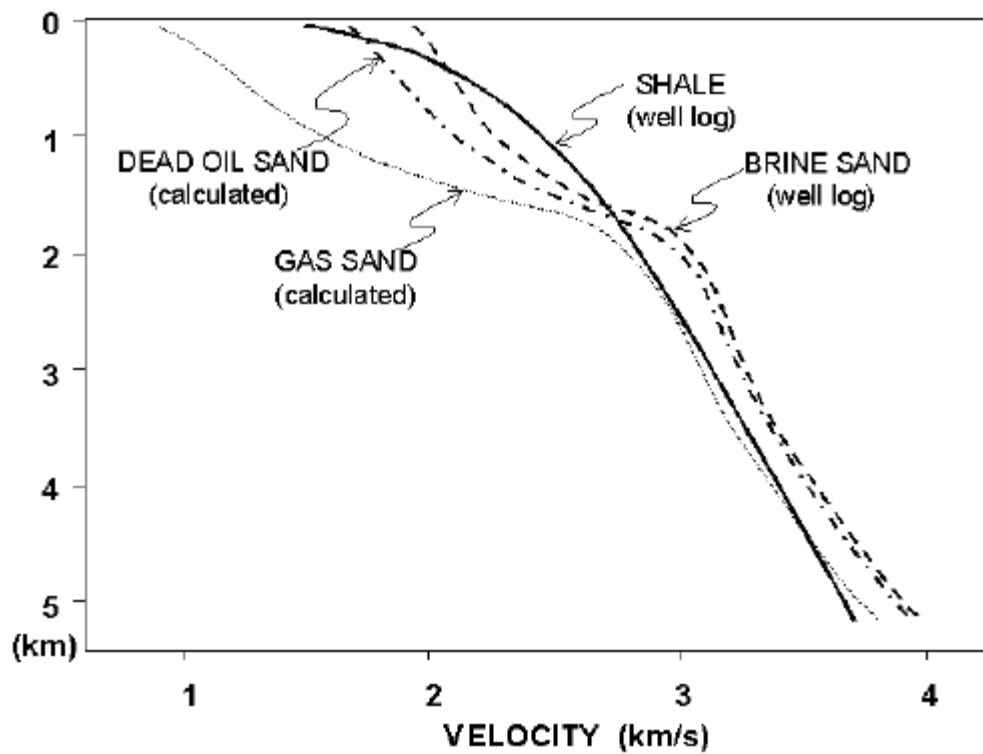

Fig. 5.2—General sand/shale velocity for the GOM under normal pressure conditions (from Batzle and Gardner[65]).

Having the compressional sonic velocity from general sand/shale velocity trend in GOM, we obtained the angle of internal friction, ϕ_f, and cohesion S_0, from Manohar's[51]shale strength correlation. These relations (Eq. 2.51 and Eq. 2.52) were developed using an extensive shale database.

5.3.2   Poisson's Ratio

Another important variable which changes with depth is Poisson's ratio. The most frequent average value of Poisson's ratio being used for rocks is 0.25, but it may cause error where depth changes. The amount of horizontal stress caused by the net overburden is a function of Poisson's ratio of the rocks.

Based on laboratory experiments, Poisson's ratio can change from well to well over 0.25, but its value is never greater than 0.5. So it is quite important to use the proper value for Poisson's ratio according to the field of study. For this reason, we have used Eaton and Eaton's Poisson ratio for deepwater Gulf of Mexico, which changes with depth (**Fig. 5.3**)[66], as shown below:

For less than 5,000 ft below mudline:

$$v = -6.089286 \times 10^{-9} z^2 + 5.7875 \times 10^{-5} z + 0.3124642857 , \quad \text{...................................... (5.3)}$$

And for 5,000 ft and greater below mudline:

$$v = -1.882 \times 10^{-10} z^2 + 7.2947129 \times 10^{-6} z + 0.4260341387 , \quad \text{...................................... (5.4)}$$
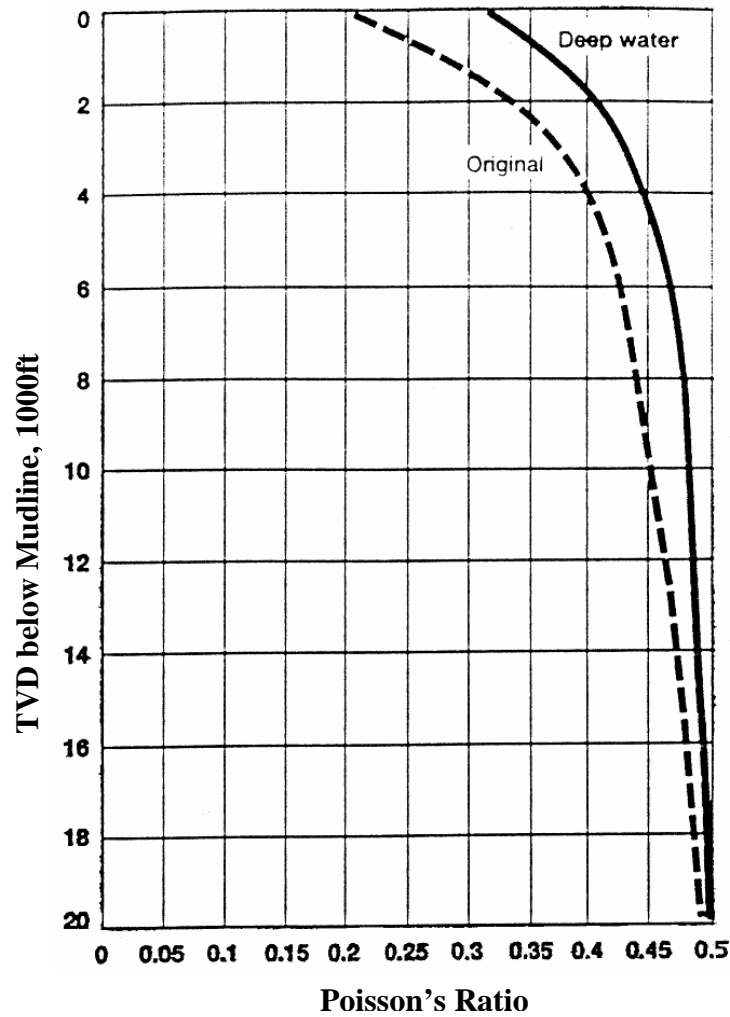
Fig. 5.3—Poisson's ratio for U.S. gulf coast and Gulf of Mexico
(from Eaton and Eaton[66]).

5.4 Failure Criteria

For this study we used modified-Lade as our failure criteria to determine the potential location of wellbore collapse.

5.5 Pore Pressure and Wellbore Pressure

To calculate the pore pressure for different depth below mudline and for different depth of water, we used generic data from deepwater GOM.

Wellbore pressure during blowout was calculated by our subroutine, which is a computational module that calculates the fluid pressure profile along wellbore. The other alternative for this subroutine is the fluid pressure profile obtained from observations or any other fluid flow simulator.

5.6 Bridging Simulation

Using modified-Lade criteria, stresses induced in the vicinity of the wellbore were compared with rock strength to determine the potential locations of fractured or collapsed intervals. We used an elastic model using a 3D generalized plane strain solution to compare the induced stresses and rock strength. We simulated bridging for water depths of 100, 1,000, 3,000, 5,000, 7,500, and 10,000 ft to determine the effect of water depth on wellbore bridging during blowout. For each water depth we performed the simulation from the seabed to the depth of 20,000 ft below mudline. Because it is assumed that the wellbore is vertical, we considered the critical angle as 90°,[27] and considered any location with breakout angle greater than this critical value as a potential part for wellbore failure or bridging.

5.6.1   Normal Faulting System: $S_H = S_V$

Fig. 5.4 shows the results of our simulation for normal faulting system, where maximum horizontal stress is equal to vertical stress.

This result shows that for the example with 10,000 ft of water depth, breakout angle is more than 90˚ anywhere lower than 3,000 ft below mudline.
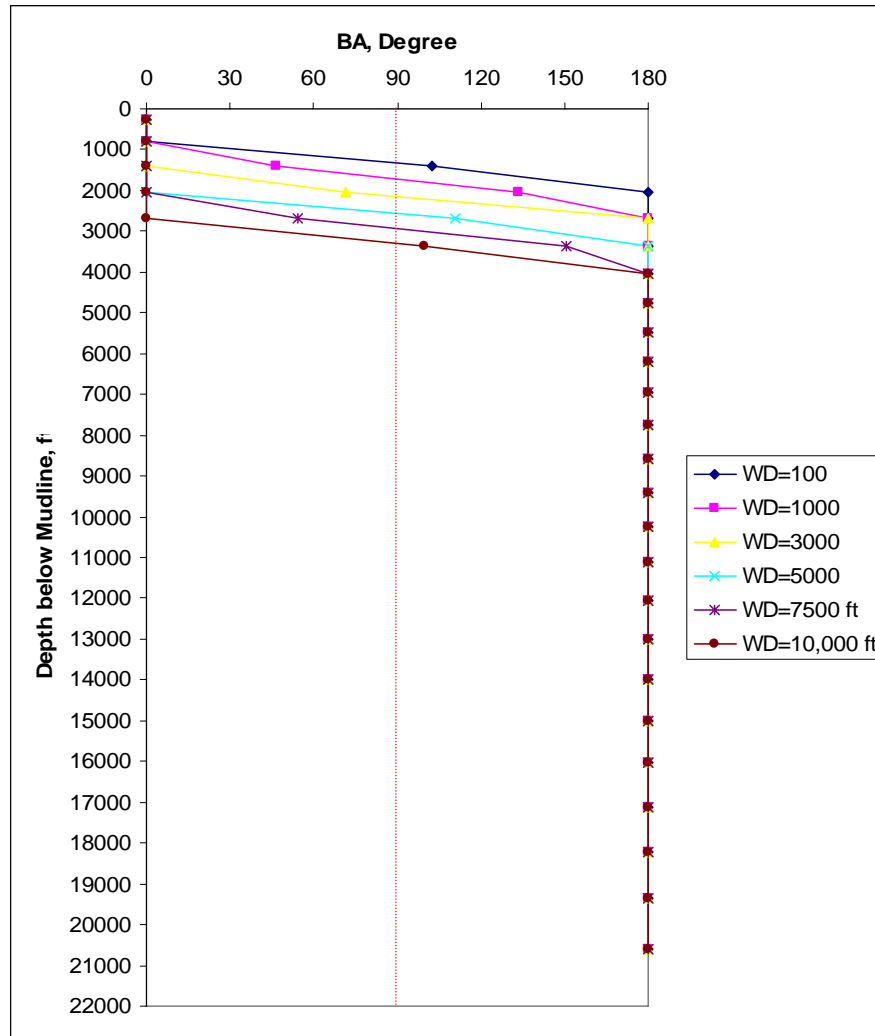
Fig. 5.4—Breakout angles during blowout for S_H=S_V.

5.6.2 *Strike-Slip Faulting System*

For this condition in our model, maximum horizontal stress is always the maximum principal stress (S_H>S_V>S_h). **Figs. A.1** to **A.9** show the relation between pore pressure, minimum horizontal stress, maximum horizontal stress, vertical stress, and wellbore pressure for different depths of water.

Results of this simulation show that in this case the critical depth in which the wellbore collapses and breakout occurs is even shallower than the previous situation, and

for 10,000 ft of water depth the breakout exceeds 90˚ everywhere below about 2,500 ft of mudline (**Fig. 5.5**).
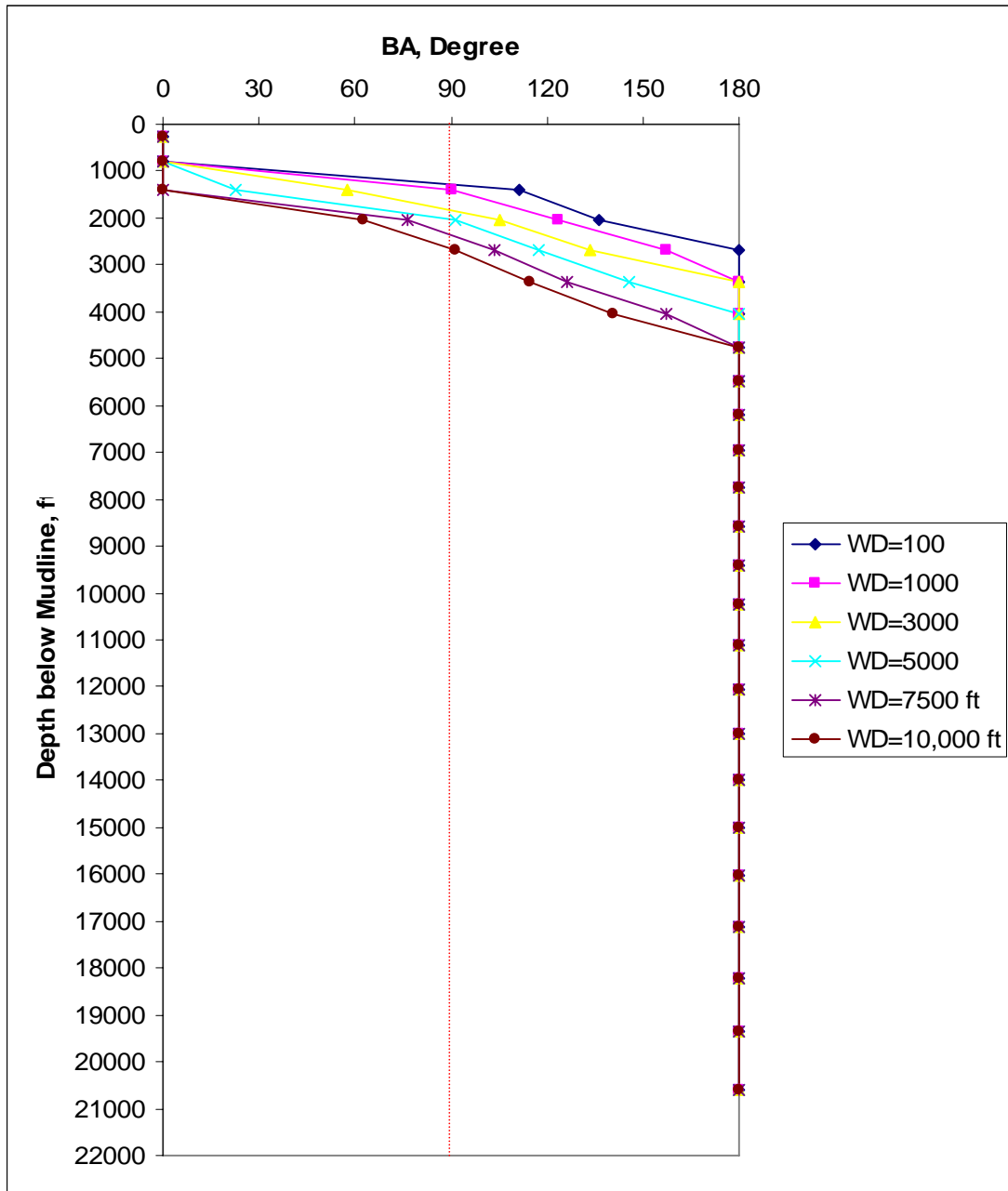

Fig. 5.5—Breakout angles during blowout for $S_H = 3.1 \times S_h - 2.1 \times P_p$.

5.6.3 $S_H=S_h$

Results of this simulation for this maximum horizontal stress show that in this case the critical depth at which the wellbore collapses and breakout occurs is deeper than the two other cases, and for 10,000 ft of water depth the breakout occurs below about 3,500 ft of mudline (**Fig. 5.6**).
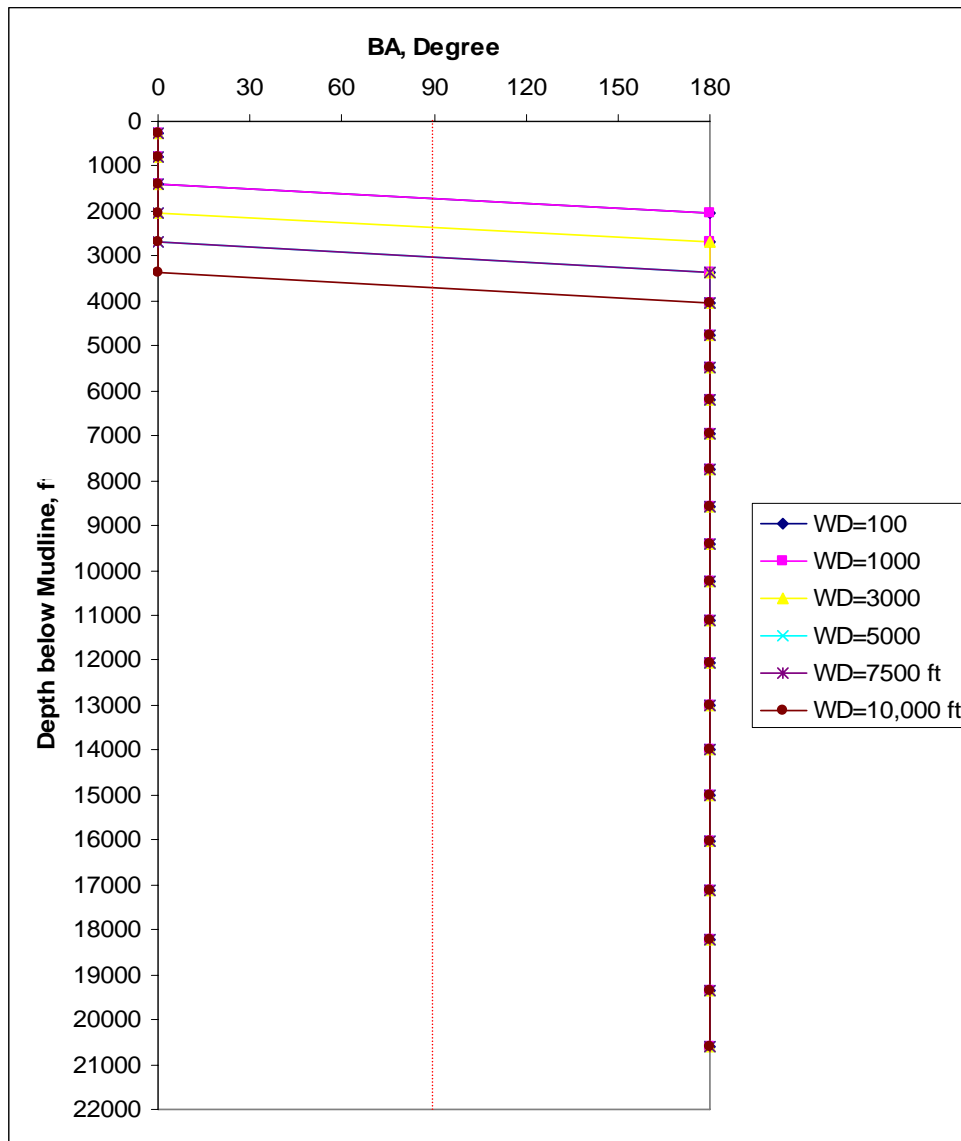

Fig. 5.6—Breakout angles during blowout for $S_H=S_h$.

CHAPTER VI

DISCUSSIONS, CONCLUSIONS, AND RECOMMENDATIONS

6.1 Wellbore Bridging Simulation for Brunei Case Study

For the field case of the bridged wellbore in Brunei, we used two sets of input data as wellbore pressure during a blowout situation. First we used pressure values based on JWCO's flowing pressure profile which they obtained from the OLGA2000 simulator.

However, as second set of pressure profiles we used our wellbore pressure subroutine, which assumes single gas flow in the wellbore during blowout to model flow along the wellbore.

Results from both simulations, demonstrate almost the same results. According to these simulations bridging is most expected within the shale formations. The reason is that the magnitude of in-situ stresses increases while the strength of the shale does not change significantly.

Also comparison between the Mohr-Coulomb and modified-Lade shows a pretty close agreement for breakout angle in blowout situation but in normal drilling situation Mohr-Coulomb shows more conservative results and it overestimates the breakout angle.

We also found that results of simulation strongly depend on the quality of available data and reliability of correlations, and having more accurate data like image logs will lead us to construct a more robust geomechanical model to get more realistic results.

6.2 Wellbore Bridging Simulation for Different Water Depths in Deepwater GOM

We investigated wellbore bridging tendencies for deepwater GOM using general trends and correlations valid for this area. Since from the previous study we concluded that breakout is most probable in shale intervals, we conducted our simulation just for shale formations.

Because the most complex factor to determine in a geomechanic model is maximum horizontal stress and we could not find any correlation for it in deepwater GOM, we considered three cases for this matter.

In the first assumption, which is valid for any normal faulting system, we assumed that maximum horizontal stress is equal to vertical stress. The second assumption is strike-slip faulting system conditions in which the maximum horizontal stress is the biggest principal stress and vertical stress is the intermediate principal stress. In the third case we assumed that the maximum horizontal stress is equal to minimum horizontal stress which was calculated from the fracture gradient for each depth.

Results of all simulations for all three categories showed that water depth delays the occurrences of critical breakout angle in the wellbore during blowout; that is, for greater depth of water, wellbore collapse occurs at greater depth below mudline. However, the depth in which collapse occurs is different for different maximum horizontal amounts.

For example, in a normal faulting system and for 10,000 ft of water, we will have wellbore bridging everywhere below about 3,000 ft below mudline. For the strike-slip faulting condition, the critical depth where the bridging starts is even shallower at about 2,500 ft below mudline. The third case, which assumes equal maximum and horizontal stress, shows that for this depth of water bridging starts from 3,500 ft below mudline.

Although these results are based on some assumptions we have made and the general trends and correlations that we used for constructing the geomechanical model, our study shows that for this case greater than 4,000 ft below mudline, wellbore bridging will occur in shale intervals if we get blowout.

In this research we studied wellbore bridging from the rock-mechanical point of view. We determined collapse potentials in the wellbore, but bridging also depends on other parameters like reservoir performance and solid transportation. As future work, adding these subroutines will make our simulator more robust.

NOMENCLATURE

C_0	=	unconfined compressive strength, kpsi
C_b	=	bulk compressibility, psi^{-1}
C_r	=	rock matrix compressibility, psi^{-1}
d	=	internal diameter, ft
E_D	=	dynamic Young's modulus, 10^6 psi
E_s	=	static Young's modulus, 10^6 psi
f	=	coefficient of friction, dimensionless
F_s	=	specific gravity (Air=1.00), dimensionless
g	=	acceleration due to gravity, ft/s^2
I_1	=	first stress invariant, psi
$I_1{}''$	=	modified first stress invariant, psi
I_3	=	third stress invariant, psi^3
$I_3{}''$	=	modified third stress invariant, psi^3
l	=	directional cosine matrix between the *(x, y, z)* coordinate system and the coordinate system *(x′, y′, z′)*,
L	=	length of pipe, ft
m	=	material parameter, dimensionless
N_{Re}	=	Reynolds number, dimensionless
p	=	pressure, psia
p_a	=	atmospheric pressure, psia
p_c	=	shut-in wellhead pressure, psia
p_{crit}	=	critical pressure, psi
p_e	=	mean effective pressure, psi
p_f	=	formation Pressure, psia
p_p	=	pore pressure, psi
p_{pn}	=	normal pore pressure, psi
p_s	=	flowing sandface pressure, psia

p_w	=	flowing wellhead pressure, psia
q	=	rate of flow, M^2cf/D @ 14.65 psia and 60°F
S_0	=	Mohr-Coulomb cohesion of the material at zero confining pressure, psi
S_1	=	cohesion-like material parameter, psi
S_h	=	minimum horizontal stress, psi
S_H	=	maximum horizontal stress, psi
S_v	=	vertical stress, psi
T	=	absolute temperature, °R
t_c	=	compressional wave transit time, μs/ft
t_f	=	compressional wave transit time of the saturating fluid rock, μs/ft
t_{ma}	=	compressional wave transit time of the matrix rock, μs/ft
t_s	=	shear-wave transit time, μs/ft
V_p	=	compressional wave sonic velocity, km/s
V_s	=	shear-wave sonic velocity, km/s
Z	=	compressibility factor, dimensionless
z	=	true vertical depth, ft
α	=	Biot constant, dimensionless
$\alpha_0 = \alpha_1 = \alpha_2 = \alpha_3$	=	constant value
γ	=	borehole inclination angle, dimensionless
Δh	=	difference in elevation, ft
$\Delta\sigma$	=	differential stress, psi
ε	=	absolute roughness, inch
ε_D	=	relative roughness, dimensionless
ε_{yy}	=	strain in y direction, dimensionless
ε_{zz}	=	strain in z direction, dimensionless
η	=	material parameter related to friction, dimensionless
η_1	=	material parameter related to friction, dimensionless

θ	=	azimuthal angle measured from the x axis, dimensionless
θ'_{zz}	=	effective axial stress, psi
μ_f	=	coefficient of internal friction and differs from the μ, coefficient of sliding friction, dimensionless
ν	=	Poisson's ratio, dimensionless
ρ_b	=	bulk density, g/cm^3
ρ_f	=	density of the saturating fluid, g/cm^3
ρ_{ma}	=	matrix density of the rock, g/cm^3
σ	=	normal stress acting on the yield plane, psi
σ_{ij}	=	total stress, psi
$\sigma_{xx} = \sigma_{yy} = \sigma_{zz}$	=	normal stresses in any Cartesian coordinates system, psi
σ_{xx}	=	normal stress in x direction, psi
σ_{zz}	=	axial stress, psi
$\sigma_{\theta\theta}$	=	tangential stress, psi
σ_1	=	maximum normal stress, psi
σ_2	=	intermediate principal stress, psi
σ_3	=	confining pressure, psi
σ_{ij}'	=	effective stress, psi
σ'_{tmax}	=	maximum effective principal stress on the tangential plane of the borehole, psi
σ'_{tmin}	=	minimum effective principal stress on the tangential plane of the borehole, psi
σ'_{rr}	=	effective radial stress, psi
$\sigma'_{\theta\theta}$	=	effective tangential stress, psi
τ	=	shear stress necessary to cause failure across a plane resisted by S_0, psi
$\tau_{xy} = \tau_{yz} = \tau_{zx}$	=	shear stresses in any Cartesian coordinates system, psi

$\tau_{\theta z}$	=	shear stress in the cylindrical coordinate system acting in the θ, z, psi
ϕ	=	rotation angle, dimensionless
ϕ_f	=	angle of internal friction, dimensionless
φ	=	porosity, dimensionless

REFERENCES

1. Adams N.J. and Kuhlman L.G.: "Case History Analyses of Shallow Gas Blowouts," paper IADC/SPE 19917 presented at the 1990 IADC/SPE Drilling Conference, Houston, 27 February - 2 March.

2. Tarr, B.A. and Flak, L.H.:"Underground Blowouts," http://www.jwco.com/technical-litterature/p06.htm, 29 December 2004.

3. Salvato, S.J. and Flak, L.H.: "Part 3-Insurance," http://www.jwco.com/technical-litterature/p03.htm, 29 December 29 2004.

4. Flak, L.H.: "Ultra-Deepwater Blowouts - How One Could Happen," http://www.boots-coots-iwc.com/references/02_Ultra-deepwater %20blowouts.htm, 29 December 29 2004.

5. Flak, L.H.: "Well Control Impacts of Deepwater Riser Margin," http://www.boots-coots-iwc.com/references/riser_margin.html, 29 December 2004.

6. Choe, J.: "Analysis of Riserless Drilling and Well-Control Hydraulics," *SPEDC*, (March 1999), 71.

7. Barnhill C.C. and Adams N.J.: "Underground Blowouts in Deep Well Drilling," paper SPE 7855 presented at the 1979 SPE Deep Drilling and Production Symposium, Amarillo, Texas, 1-3 April.

8. Skalle, P. and Podio, A.L.: "Trends Extracted From 800 Gulf Coast Blowouts During 1960-1996," paper IADC/SPE 39354 presented at the 1998 IADC/SPE Drilling Conference, Dallas, 11 March.

9. Skalle, P., Jinjun, H. and Podio, A.L.: "Killing Methods and Consequences of 1120 Gulf Coast Blowouts During 1960-1996," paper SPE 53974 presented at the 1999 SPE Latin American and Caribbean Petroleum Engineering Conference, Caracas, Venezuela, 21–23 April.

10. Wylie, W.W. and Visram, A.S.: "Drilling Kick Statistics," paper IADC/SPE 19914 presented at the 1990 IADC/SPE Drilling Conference, Houston, 27 February - 2 March.

11. Adams N.J. and Kuhlman L.G.: "Shallow Gas Blowout Kill Operations," paper SPE 21455 presented at the Middle Eest Oil Show, Bahrain, 16-19 November.

12. "Wellbore Stability Guidelines," http://www.kingdomdrilling.co.uk/problem/adobe/ WSG01.pdf, 29 December 2004.

13. El-Sayed, A-A.H.: "Maximum Allowable Production Rates From Openhole Horizontal Wells," paper SPE 21383 presented at the 1991 SPE Middle East Oil Show, Bahrain, 16-19 November.

14. Maury, V. and Guenot A.: "Practical Advantages of Mud Cooling Systems for Drilling," paper SPE/IADC 25732 presented at the 1993 SPE/IADC Drilling Conference, Amsterdam, 23-25 February.

15. Van den Hoek, P.J., Hertogh, G.M.M., Kooijman, A.P., de Bree, Ph. and Kenter, C.J.: "New Concept of Sand Production Prediction: Theory and Laboratory Experiments," paper SPE 36418 presented at the 1996 SPE Annual Technical Conference, Denver, 6-9 October.

16. Detournay, E. and Cheng, A.H.-D. "Fundamentals of Poroelasticity, " *Comprehensive Rock Engineering Principles, Practice and Projects Vol. II, Analysis and Design Methods*, C. Fairhurst (ed.), Pergamon Press, Oxford (1993) Chap. 5, 113-171.

17. *Mining Engineering Handbook*, Hartman, H.L., SME Littleton, CO., (1992).

18. Budiningsih, Y., Hareland, G., Boonyapaluk, P. and Guo, B.: "Correct Production Rates Eliminate Sand Production in Directional Wells," paper SPE 29291 presented at the 1995 SPE Asia Pacific Oil & Gas Conference, Kuala Lumpur, 20-22 March.

19. Maury, V. and Zurdo, C.: "Drilling-Induced Lateral Shifts Along Pre-Existing Fractures: A Common Cause of Drilling Problems," *SPEDC* (March 1996) 17.

20. Hill, R.: *The Mathematical Theory of Plasticity*, University Press, Oxford (1950).

21. Kachanov, L.M., *Foundations of the Theory of Plasticity*, Elsevier, New York (1971).

22. Gray, K.E.: "Some Updates for Fracture, Lost Circulation, Leak-Off, and Pore Pressure Technology," paper AADE 01-NC-HO-45 presented at the 2001 AADE National Drilling Conference, Houston, 27-29 March.

23. Awal, M.R., Khan, M.S., Mohiuddin, M.A., Abdulraheem, A. and Azeemuddin, M.: "A New Approach to Borehole Trajectory Optimization for Increased Hole Stability," paper SPE 68092 presented at the 2001 SPE Middle East Oil Show, Bahrain, 17-20 March.

24. Van Oort, E., Nicholson, J., and D'Agostino, J.: "Integrated Borehole Stability Studies: Key to Drilling at the Technical Limit and Trouble Cost Reduction," paper SPE/IADC 67763 presented at the 2001 SPE/IADC Drilling Conference, Amsterdam, 27 February–1 March.

25. Mohiuddin, M.A., Awal, M. R., and Khan, K.: "A New Diagnostic Approach to Identify the Causes of Borehole Instability Problems in an Offshore Arabian Field," paper SPE 68095 presented at the 2001 SPE Middle East Oil Show, Bahrain, 17–20 March.

26. Garrouch, A.A. and Ebrahim, A.S.: "Assessment of the Stability of Inclined Wells," paper SPE 68861 presented at 2001 SPE Western Regional Meeting, Bakersfield, California, 26-30 March.

27. Moos, D.: "Wellbore Stability in Deep Water—Handling Geomechanical Uncertainty," paper AADE 01-NC-HO-43 presented at the AADE 2001 National Drilling Conference, Houston, 27 - 29 March.

28. Maury, V. and Sauzay J-M.: "Borehole Instability: Case Histories, Rock Mechanics Approach, and Results," paper SPE/IADC 16051 presented at the 1987 IADC/SPE Drilling Conference, New Orleans, 15-18 March.

29. Adams, A.J. and Hodgson, T.: "Calibration of Casing/Tubing Design Criteria by Use of Structural Reliability Techniques," *SPEDC* (March 1999) 14.

30. Andersen, L.B. and Aven, T.: "On Risk Interpretation and the Levels of Detail in Modeling Quantitative Blowout Risk," paper SPE 35967 presented at the 1996 International Conference on Health, Safety & Environment, New Orleans, 9-12 June.

31. Frydman, M. and Fontoura, S.A.B.: "Modeling Aspects of Wellbore Stability in Shales," paper SPE 69529 presented at the 2001 SPE Latin American and Caribbean Petroleum Engineering Conference, Buenos Aires, 25–28 March.

32. *The SINTEF Offshore Blowout Database,* http://www.sintef.no/units/indman/sipaa /prosjekt/blowout.html, 31 December 2004.

33. Willson, S.M., Last, N.C., Zoback, M.D. and Moos, D.: "Drilling in South America : A Wellbore Stability Approach for Complex Geologic Conditions, " paper SPE 53940 presented at the 1999 SPE Latin American and Caribbean Petroleum Engineering Conference, Caracas, 21–23 April.

34. Yarlong, W. and Lu, B.: "A Coupled Reservoir-Geomechanics Model and Applications to Wellbore Stability and Sand Prediction," paper SPE 69718-MS presented at the 2001 SPE International Thermal Operations and Heavy Oil Symposium, Margarita Island, Venezuela, March 12-14.

35. Moos, D. and Zoback, M.D.: "Feasibility Study of the Stability of Openhole Multilaterals, Cook Inlet, Alaska," paper SPE 52186-MS presented at 1999 SPE Mid-Continent Operations Symposium, Oklahoma City, Oklahoma, 28-31 March.

36. Wiprut, D. and Zoback, M.D.: "Constraining the Full Stress Tensor in the Visund Field, Norwegian North Sea: Application to Wellbore Stability and Sand Production," *Int'l . J. Rock Mech. & Mining Science* (2000) **37**, 317.

37. Hemphill, T. and Tare, U.: "Extensive Pre-Well Integrated Modeling Aids in Successful Drilling of Challenging Well: A Case Study," paper AADE 01-NC-HO-18 presented at 2001 AADE National Drilling Conference, Houston, Texas, 27-29 March.

38. Ghassemi A., Diek, A. and Santos, H.: "Effects of Ion Diffusion and Thermal Osmosis on Shale Deterioration and Borehole Instability," paper AADE 01-NC-HO-

40 presented at 2001 AADE National Drilling Conference, Houston, Texas, 27-29 March.

39. Terzaghi, K.V.: *Theoretical Soil Mechanics*, John Wiley and Sons Inc., New York (1943) 51.

40. Biot, M.A.: "Theory of Elasticity and Consolidation for a Porous Anisotropic Solid," *J. of Applied Physics Research* (1955) **26**, 182.

41. Fjaer, E., Holt, R.M., and Horsrud, P.: *Petroleum Related Rock Mechanics*, Elsevier, Amsterdam (1992).

42. Desai, C.S. and Christian, J.T.: *Numerical Methods in Geotechnical Engineering*, McGraw-Hill, New York (1977).

43. Economides, M.J. and Nolte, K.G.: *Reservoir Simulation*, Schlumberger Educational Services, Houston, (1989).

44. Jaeger, J.C. and Cook, N.G.W: *Fundamentals of Rock Mechanics*, Chapman and Hall, London (1979).

45. Goodman, R.E.: *Introduction to Rock Mechanics*, John Wiley & Sons, New York (1989).

46. Ewy, R.T.: "Wellbore Stability Prediction by Use of a Modified Lade Criterion," paper SPE 56862 presented at 1998 SPE/ISRM Eurock, Trondheim, 8-10 July.

47. Desai C.S. and Gallager R.H.: *Mechanics of Engineering Materials,* Wiley, New York (1984).

48. Zheng, Z.: "Integrated Borehole Stability Analysis Against Tradition," paper SPE 47282 presented at the 1998 SPE/ISRM Eurock '98, Trondheim, 8-10 July.

49. Gardner, G.H.F., Gardner, L.W., and Gregory, A.R.:"Formation Velocity and Density – The Diagnostic Basics for Stratigraphic Traps," *Geophysics* (December 1974) **39**, 770.

50. Lacy, L.L.: "Dynamic Rock Mechanics Testing for Optimized Fracture Designs," paper SPE 38716 presented at the 1996 SPE Annual Technical Conference and Exhibition, San Antonio, Texas, 5-8 October.

51. Manohar, L.: "Shale Stability: Drilling Fluid Interaction and Shale Strength," paper SPE 54356 presented at the 1999 SPE Latin American and Caribbean Petroleum Engineering Conference, Caracas, Venezuela, 21-23 April.

52. Hills, R.R.: "Coupled Changes in Pore Pressure and Stress in Oil Fields and Sedimentary Basins," *Petroleum Geoscience*, (2001) **7,** 419.

53. *Log Interpretation Principles/Applications*, Schlumberger, Houston (1996).

54. Khaksar, A., Warrington, A.H., Magee, M.E., Burgdorff, K.L. and Castillo, D.A.: "Coupled Pore Pressure and Wellbore Breakout Analysis in the Complex Papua New Guinea Fold Belt Region," paper SPE 88607 presented at the 2004 SPE Asia Pacific Oil and Gas Conference, Perth, Australia, 18-20 October.

55. Cullender, M.H., and Smith, R.V.: "Practical Solution of Gas-Flow Equations for Wells and Pipelines with Large Temperature Gradients," paper SPE 696-G presented at the 1956 Petroleum Branch Fall Meeting, Los Angeles, 11-17 October.

56. Salvadori, M.G., and Baron, M.L.: *Numerical Methods in Engineering*, Prentice-Hall Inc., New York (1952).

57. Moody, L.F.: "Friction Factors for Pipe Flow" *Trans*. ASME (1994) **66**, 666, 671.

58. Colebrook, C.F.: "Turbulent Flow in Pipes, with Particular Reference to the Transition Region Between the Smooth and Rough Pipe Laws," *J. Inst. Civil Engr.*, London (1938-1939) **11**, No. 1, 133.

59. Well Flow Dynamics, "Well SWA-184 ST1 Blowout-Hydraulics Blowout & Kill Evaluation," Report, 2002: Billingstad, NORWAY.

60. Breckels, I.M. and van Eekelen, H.A.M.: "Relationship Between Horizontal Stress and Depth in Sedimentary Basin," *JPT*, (1982) **34,** 2191.

61. Lindsay, R.O., and Foster, R.K.: "Correcting a False Assumption – Offshore Brunei," *The Leading Edge*, (June 2002) **21,** 536.

62. Zhang, J.J., Rai, C.S., and, Sondergeld, C.H.: "Mechanical Strength of Reservoir Materials: Key Information for Sand Prediction," paper SPE 62499 presented at 1998 SPE Annual Technical Conference and Exhibition, New Orleans, Louisiana, 27-30 September.

63. Eaton, B. A.: "Fracture Gradient Predictions and Its Application in Oil Field Operations," *JPT*, (1969) **21,** 1353.

64. Zoback, M. D., Barton, C. A., Brudy, M., Castillo, D. A., Finkbeiner, *et al.*: "Determination of Stress Orientation and Magnitude in Deep Wells," *International J. of Rock Mechanics and Mining Sciences* (2003) **40,** 1049.

65. Batzle, M.L. and Gardner, M.H.: "Lithology and Fluids: Seismic models of the Brushy Canyon Formation, West Texas, " *Fine-Grained Turbidite Systems*, A.H. Bouma, and C.G. Stone, *AAPG Memoir 72 - SEPM Spec. Pub. 68*, AAPG, Tulsa, Oklahoma, U.S.A. (2000).

66. Eaton, B.A. and Eaton, T.L.: "Fracture Gradient Prediction for New Generation," *World Oil* (1997) **418,** No. 10, 93.

APPENDIX A
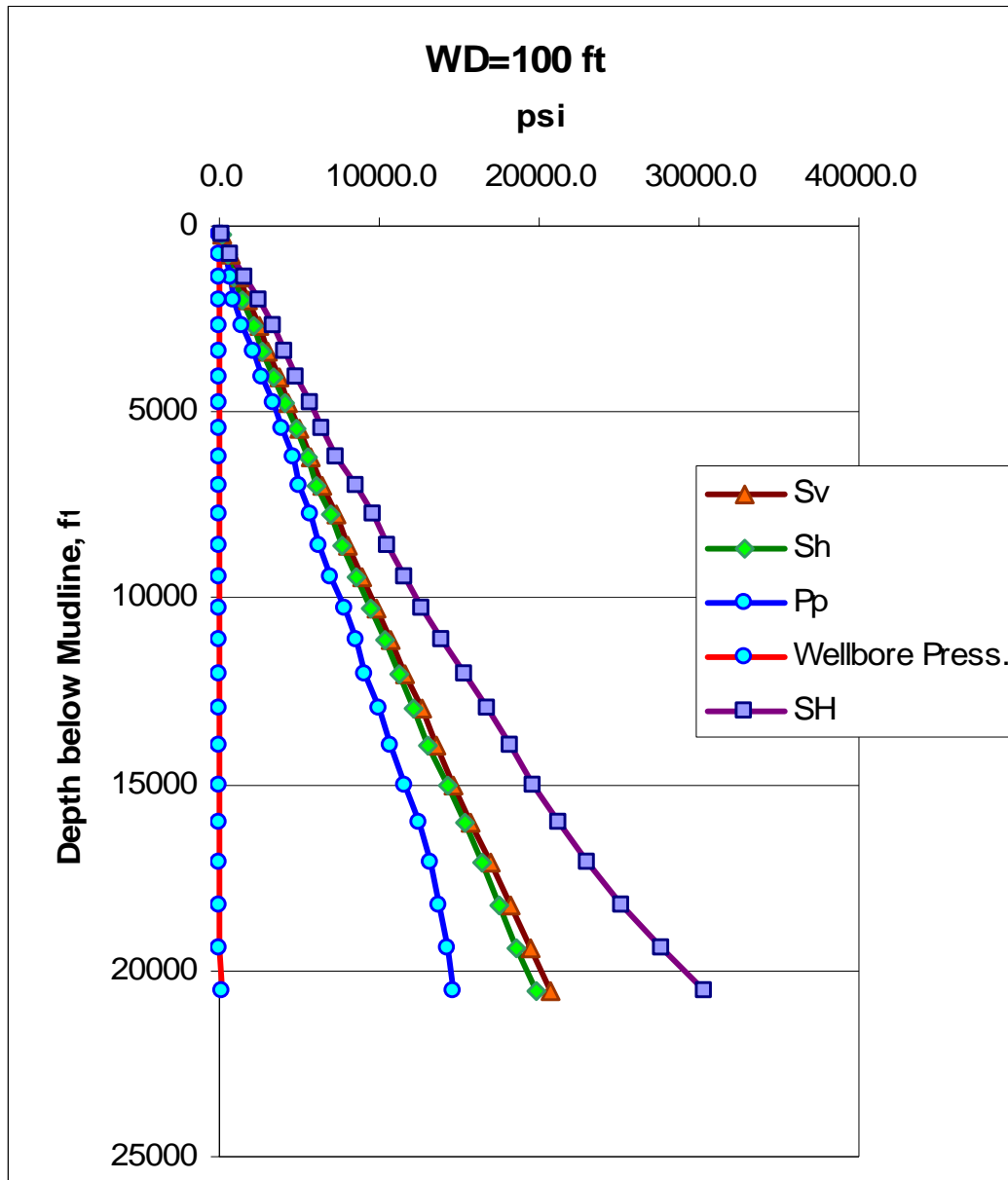
Fig. A.1—In-situ stresses, pore pressure and wellbore pressure for strike-slip faulting case and WD=100 ft.
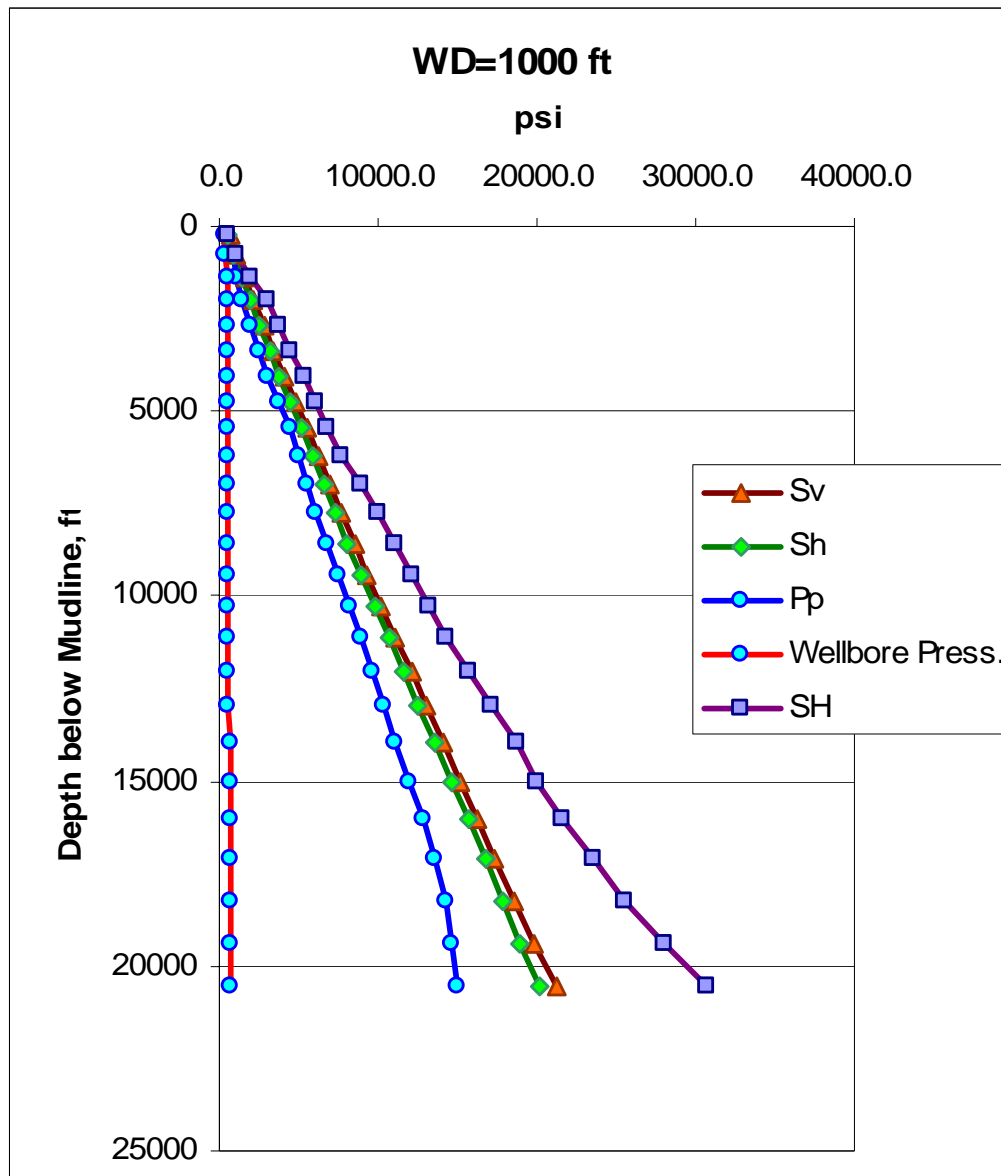
Fig. A.2—In-situ stresses, pore pressure and wellbore pressure for strike-slip faulting case and WD=1000 ft.
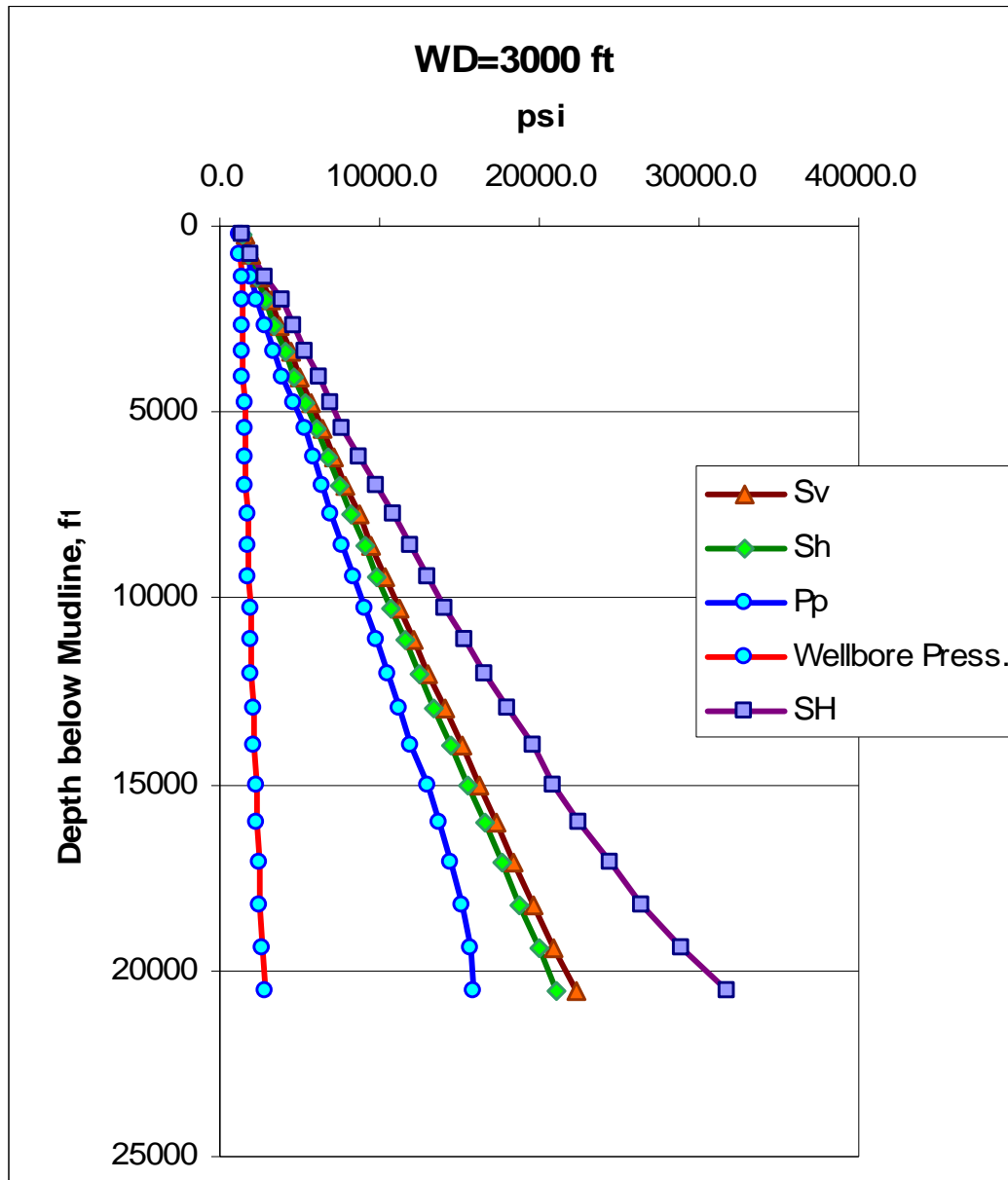
Fig. A.3—In-situ stresses, pore pressure and wellbore pressure for strike-slip faulting case and WD=3000 ft.
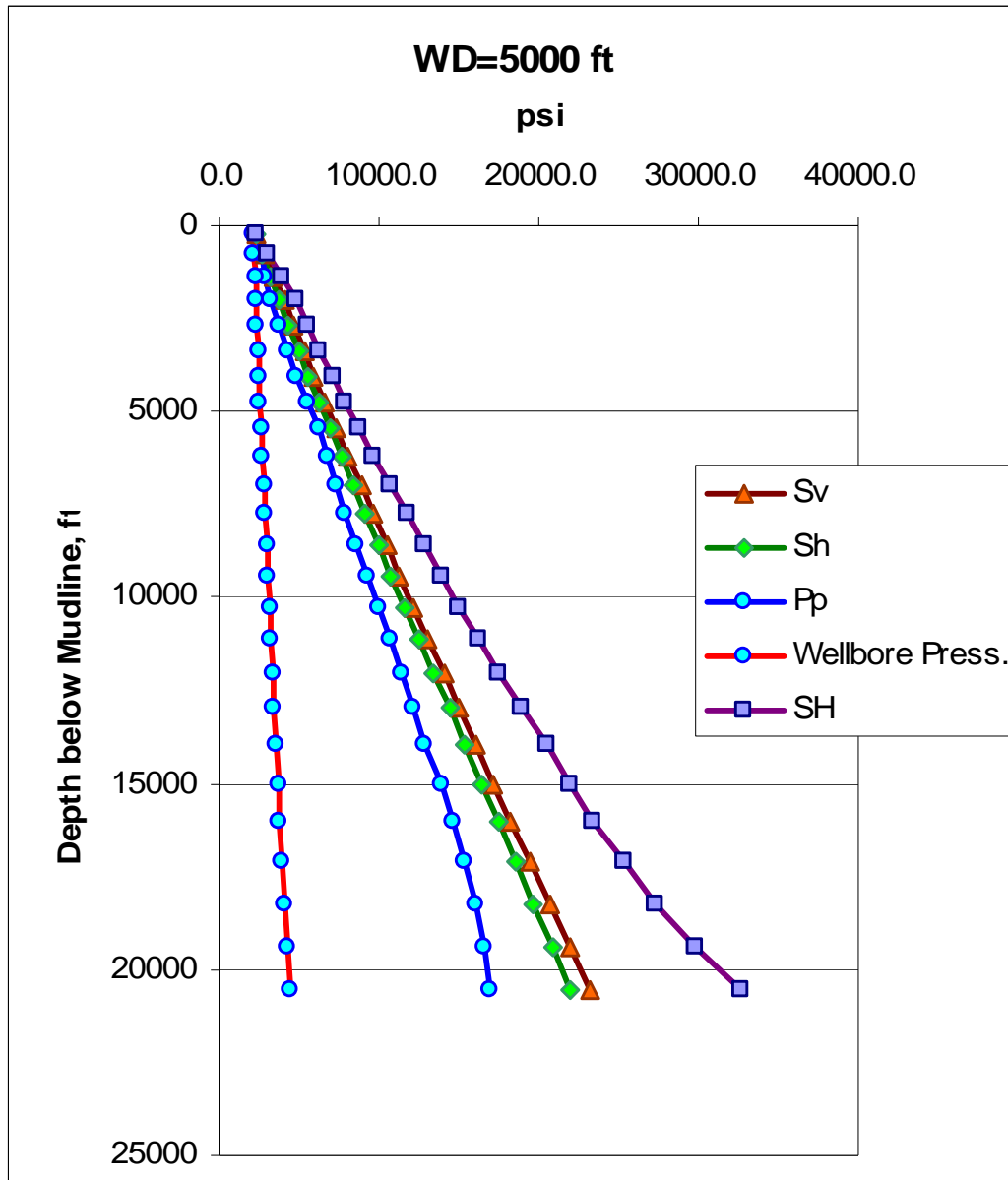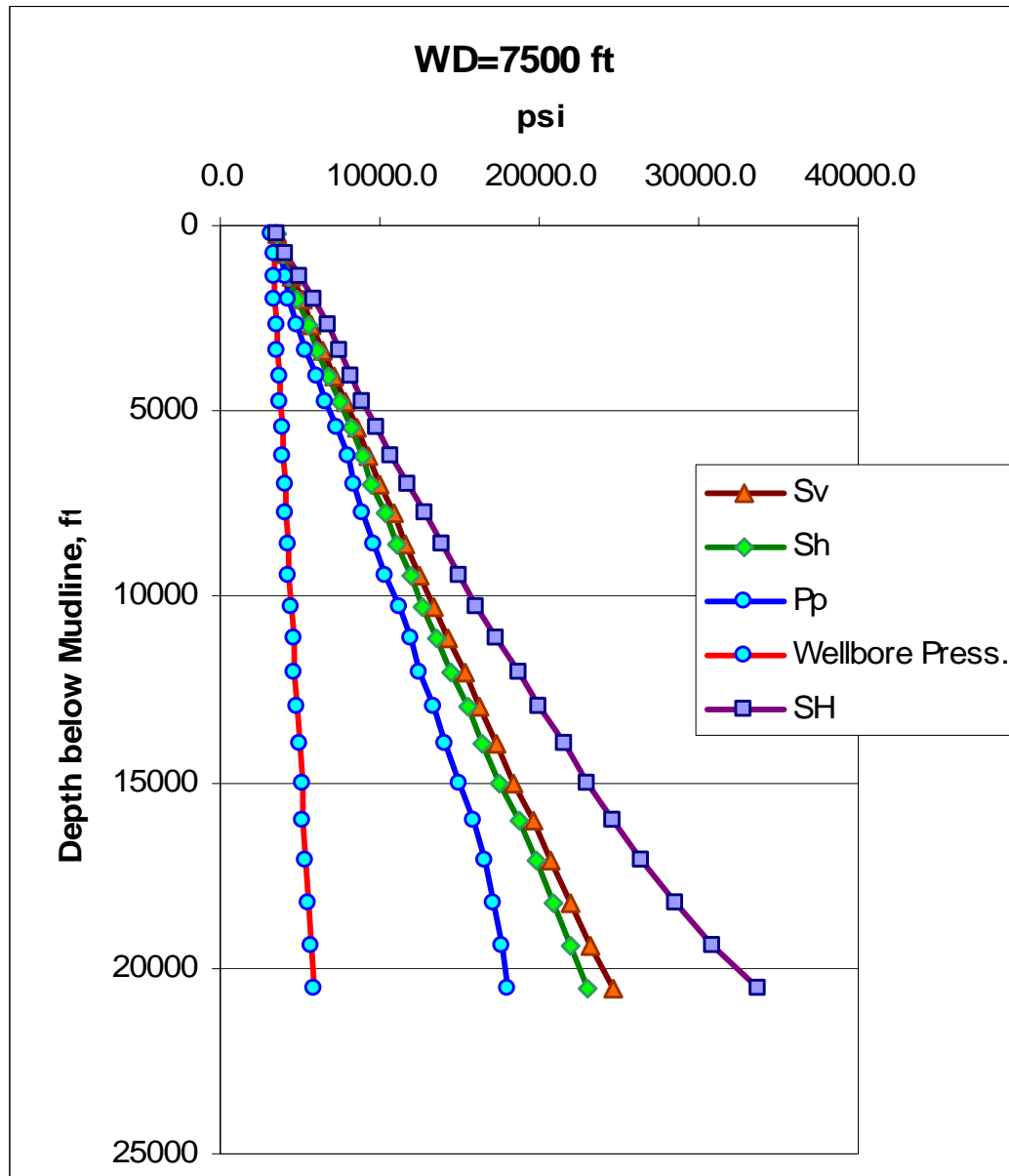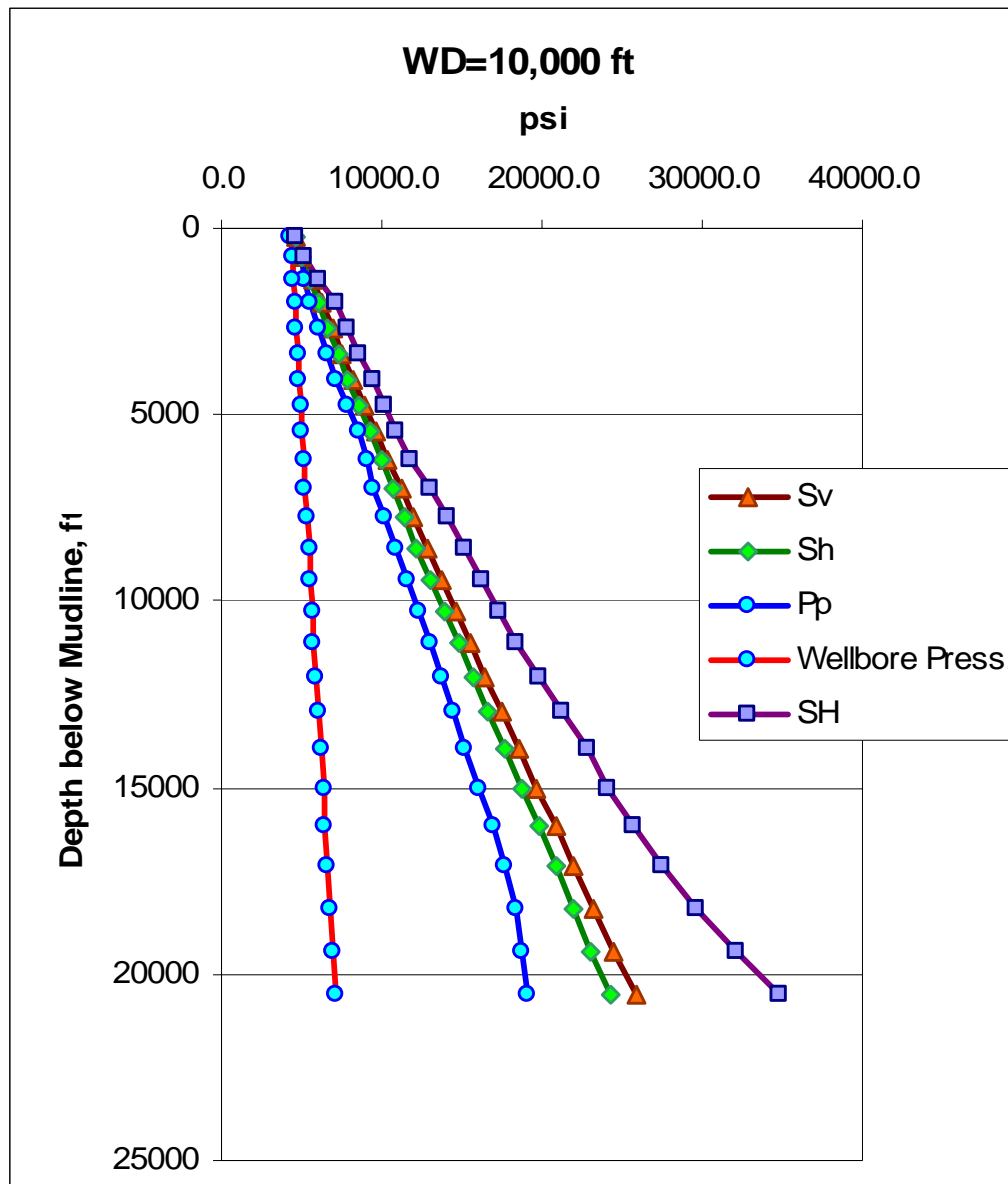
Fig. A.4—In-situ stresses, pore pressure and wellbore pressure for strike-slip faulting case and WD=5000 ft.
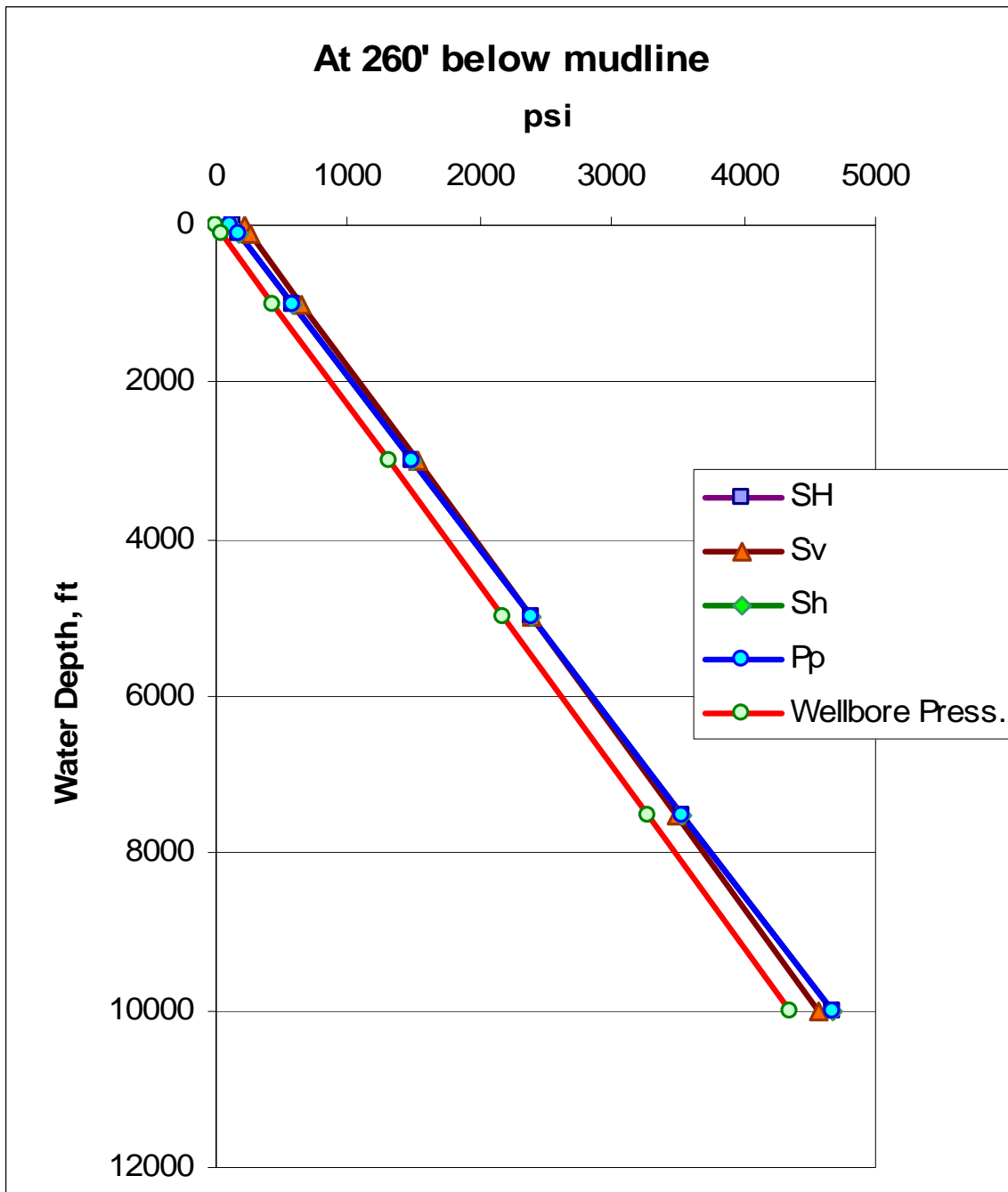
Fig. A.5—In-situ stresses, pore pressure and wellbore pressure for strike-slip faulting case and WD=7500 ft.

Fig. A.6—In-situ stresses, pore pressure and wellbore pressure for strike-slip faulting case and WD=10,000 ft.

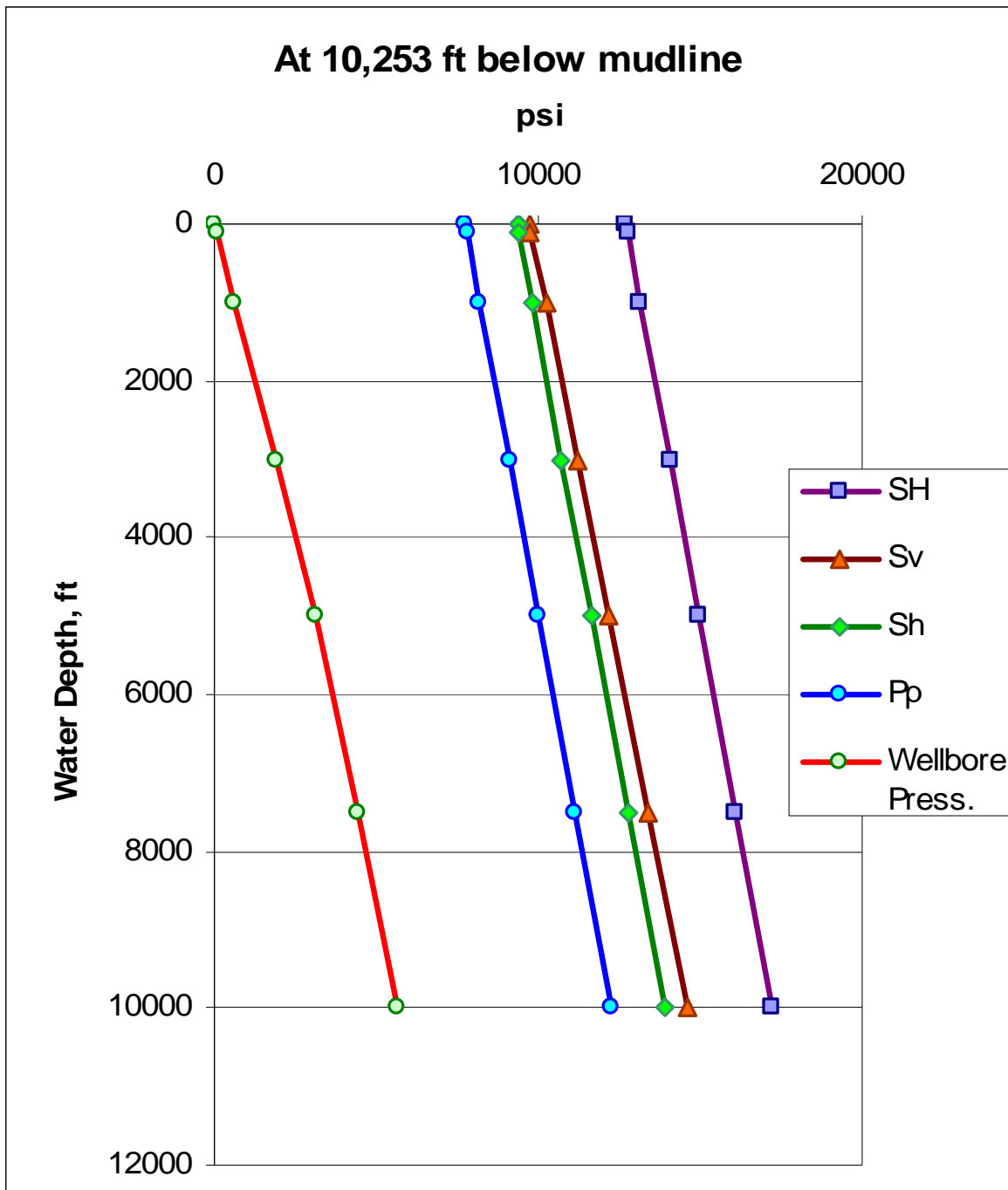**Fig. A.7**—In-situ stresses, pore pressure and wellbore pressure for strike-slip faulting case and 260 ft below mudline.

Fig. A.8—In-situ stresses, pore pressure and wellbore pressure for strike-slip faulting case and 10,253 ft below mudline.
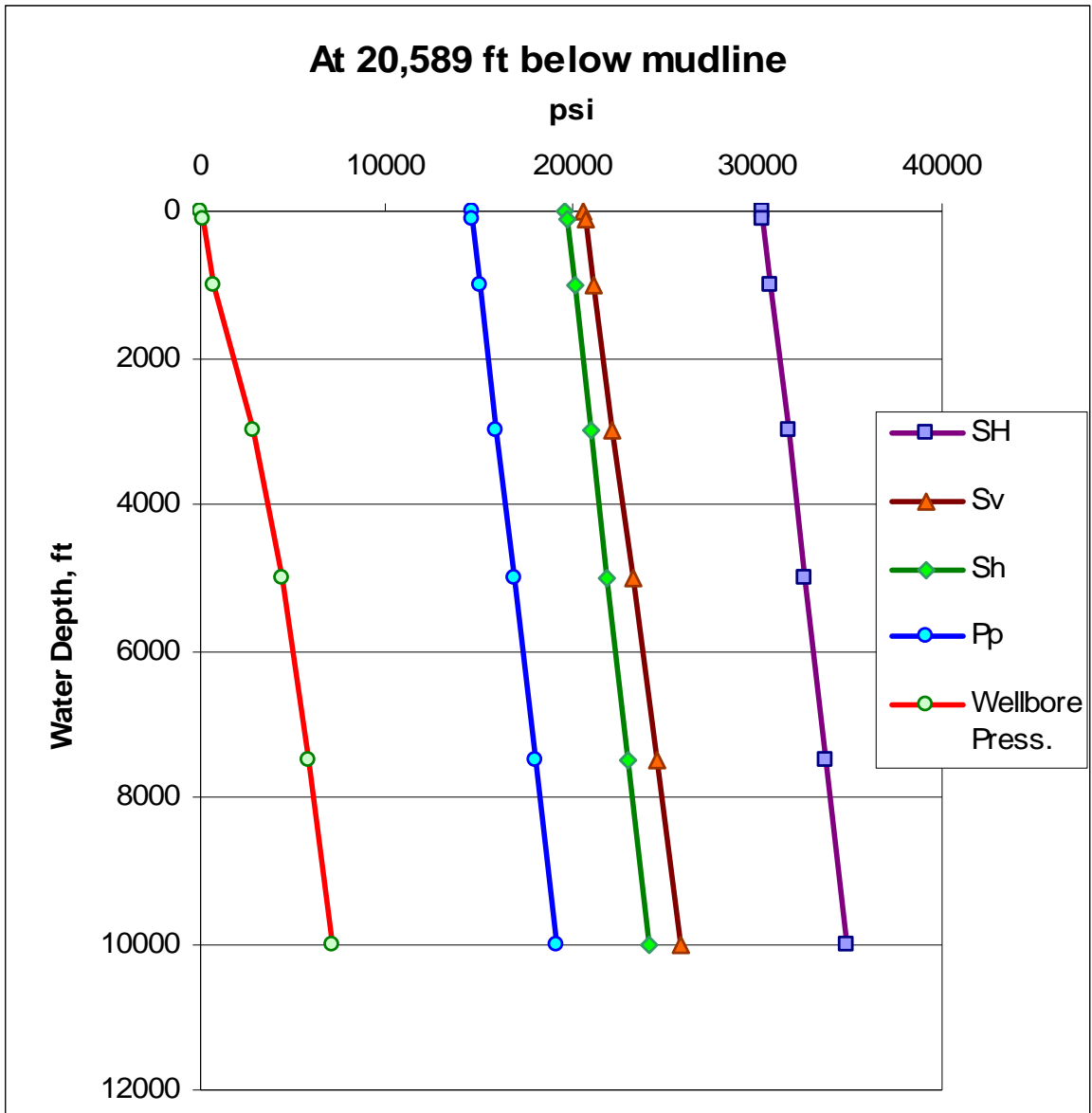
Fig. A.9—In-situ stresses, pore pressure and wellbore pressure for strike-slip faulting case and 20,589 ft below mudline.

VITA

Name: Babak Akbarnejad Nesheli

Place of Birth: Tehran, Iran

Address: Azadi Street, Shahid Akbari Ave., Daneshgah Tehran
Complex, Block C, Apt. # 2, 1458758511
Tehran, Iran

Education: Tehran University
Tehran, Iran
B.S. in Mining Engineering (2002)

Texas A&M University
College Station, Texas, USA
M.S. in Petroleum Engineering (2006)